

Discrete-Time Complementary Filters for Attitude and Position Estimation: Design, Analysis and Experimental Validation

José F. Vasconcelos, *Student Member, IEEE*, Bruno Carneira, Carlos Silvestre, *Member, IEEE*, Paulo Oliveira, *Member, IEEE*, and Pedro Batista, *Student Member, IEEE*

Abstract—This paper develops a navigation system based on complementary filtering for position and attitude estimation, with application to autonomous surface crafts. Using strapdown inertial measurements, vector observations, and global positioning system (GPS) aiding, the proposed complementary filters provide attitude estimates in Euler angles representation and position estimates in Earth frame coordinates, while compensating for rate gyro bias. Stability and performance properties of the proposed filters under operating conditions usually found in oceanic applications are derived, and the tuning of the filter parameters in the frequency domain is emphasized. The small computational requirements of the proposed navigation system make it suitable for implementation on low-power hardware and using low-cost sensors, providing a simple yet effective multirate architecture suitable to be used in applications with autonomous vehicles. Experimental results obtained in real time with an implementation of the proposed algorithm running on-board the DELFIMx catamaran, an autonomous surface craft developed at ISR/IST for automatic marine data acquisition, are presented and discussed.

Index Terms—Complementary filters, navigation systems, strapdown systems, time-varying systems.

NOMENCLATURE

The notation adopted is fairly standard. The Gaussian distribution with mean μ and variance σ^2 is denoted as $\mathcal{N}(\mu, \sigma^2)$. The set of $n \times m$ matrices with real entries is denoted as $\mathbb{M}(n, m)$. Column vectors and matrices are denoted respectively by lowercase and uppercase boldface type, e.g., \mathbf{s} and \mathbf{S} . The transpose of a vector or matrix will be indicated by a prime, and trailing subscripts $\{x, y, z\}$ denote the vector components, $\mathbf{s} = [s_x \ s_y \ s_z]'$. Leading subscripts and superscripts identify the coordinate system of a quantity, e.g., ${}^E\mathbf{s}$ is represented in coordinate frame $\{E\}$, and ${}^E_B\mathbf{R}$ is a rotation matrix that transforms

the vector representation ${}^B\mathbf{s}$ into ${}^E\mathbf{s}$ by means of the linear operation ${}^E\mathbf{s} = {}^E_B\mathbf{R}{}^B\mathbf{s}$. Position, velocity, and acceleration are denoted respectively by \mathbf{p} , \mathbf{v} , and \mathbf{a} , and the angular velocity of the vehicle expressed in body coordinates is represented by $\boldsymbol{\omega}$. The nominal, the measured, and the estimated quantity \mathbf{s} are denoted by $\bar{\mathbf{s}}$, \mathbf{s}_r , and $\hat{\mathbf{s}}$, respectively, and $\|\mathbf{s}\|$ denotes the Frobenius norm. Discrete-time quantities are characterized by the time index k subscript. The identity and zero matrices are, respectively, denoted as \mathbf{I} and $\mathbf{0}$. The dimensions of the vector and matrices are clear from the context. In general, the vectors are elements (or a concatenation of elements) of \mathbb{R}^3 .

I. INTRODUCTION

MARINE biologists, oceanographers, and other ocean researchers depend increasingly on technology to conduct their studies on time and space scales that suit the phenomena under study. A particular field of interest is structural health monitoring, which plays nowadays a major role in maintaining large critical semi-submerged infrastructures, like bridges and breakwaters. Most of these structures are exposed to harsh environments and heavy loads, and hence are designed under the proviso that maintenance works will be required during the structure's life. However, surveillance operations are complex and expensive, and great emphasis is being placed on the use of autonomous vehicles as a quality and cost-effective alternative.

Autonomous surface crafts exhibit a high degree of operational reliability in the presence of dynamic, uncertain environments, and challenging scenarios. The autonomous catamaran DELFIMx, built at IST-ISR and displayed in Fig. 1, was designed for automatic marine data acquisition for risk assessment in semi-submerged structures [1], allowing for the access to remote and confined locations in a systematic way, as required for precise sonar data acquisition. To successfully execute its mission, the catamaran is required to have a reliable on-board navigation system based on low-power consumption, inexpensive hardware, capable of efficiently integrating the information from inertial and aiding sensor suites.

This paper presents the development of a global positioning system (GPS) aided inertial measurement unit (IMU) using complementary filters. The problem of accurate position and attitude estimation is addressed by exploiting information provided by the vehicle sensor suite over distinct, yet complementary frequency regions. Namely, inertial measurements from rate gyros and accelerometers are merged with the linear

Manuscript received July 21, 2008; revised February 13, 2009. Manuscript received in final form January 10, 2010. First published February 18, 2010; current version published December 22, 2010. Recommended by Associate Editor S. Kim. This work was supported in part by Fundação para a Ciência e a Tecnologia (ISR/IST pluriannual funding) through the POS_Conhecimento Program that includes FEDER funds and by the project MEDIREs from ADI and project PDCT/MAR/55609/2004—RUMOS of the FCT. The work of J. F. Vasconcelos and P. Batista was supported by the Ph.D. Student Scholarships SFRH/BD/18954/2004 and SFRH/BD/24862/2005, respectively, from the Portuguese FCT POCTI Programme.

The authors are with the Institute for Systems and Robotics (ISR), Instituto Superior Técnico (IST), 1049-001 Lisbon, Portugal (e-mail: jfvasconcelos@isr.ist.utl.pt; bcarreira@isr.ist.utl.pt; cjs@isr.ist.utl.pt; pjcro@isr.ist.utl.pt; pbatista@isr.ist.utl.pt).

Color versions of one or more of the figures in this paper are available online at <http://ieeexplore.ieee.org>.

Digital Object Identifier 10.1109/TCST.2010.2040619



Fig. 1. DELFIMx autonomous surface craft (length: 4.5 m; width: 2.45 m; mass: 300 Kg).

position available from a low-cost GPS receiver, and with Earth's magnetic field observations. The proposed filters are required to yield accurate position and attitude estimates, that will be central to stabilize the platform and support the implementation of reliable trajectory tracking and path following control strategies [2].

While a unified error analysis for inertial navigation system (INS) can be found in the literature [3], the choice of filtering architectures ranges from classical methodologies to recently proposed approaches [4]. The extended Kalman filter (EKF) is one of the most well known and widely adopted filtering algorithms, see [4]–[8], and the unscented Kalman filter (UKF) has been put forth as an alternative to the EKF [4], [9], [10], which numerically approximates the mean and covariance of the state estimate parametrized in Euclidean spaces. More recently, there has been an increasing interest in the design of nonlinear observers that are theoretically stable and yield explicit regions of attraction [11]–[16].

The navigation system proposed in this work is based on the complementary filtering theory, deeply rooted in the work of Wiener [17]: an unknown signal can be estimated using corrupted measurements from one or more sensors, whose information naturally stands in distinct and complementary frequency bands [18]–[21]. The minimum mean-square estimation (MMSE criteria) error was first solved by Wiener [17], assuming that the unknown signal had noise-like characteristics, which usually does not fit the signal description. Complementary filtering explores the sensor redundancy to successfully reject measurement disturbances in complementary frequency regions, without distorting the signal. The slight loss of performance in complementary filters, due to ignoring noise stochastic description, is beneficial in the presence of irregular measures that occur out of the expected variance, as convincingly argued in [18].

Complementary filters have been widely used in the past in sensor fusion problems. The frequency domain formulation, and the simple filter structure, allow for straightforward implementation without requiring high performance signal processing hardware, see [22], [23], and references therein. These algorithms are highly appealing in face of limited computational resources, and are adopted in navigation systems for autonomous vehicles such as oceanic crafts [24]–[26],

model-scale helicopters [27], and autonomous aircrafts [28], [29] due to the algorithm simplicity and reliability in practical implementations.

The derivation of the proposed attitude and position complementary filters is focused on the stability, performance, and practical implementation of the filtering algorithm. The complementary filter structure, shown in Fig. 2, consists of an attitude filter and a position filter. Formulated in discrete-time, the attitude filter entries are the rate gyro readings, corrupted by bias, and a snapshot attitude reconstruction based on vector observations, such as magnetic-field and pendular readings. The position filter resorts to accelerometers readings and to GPS, and estimates velocity in body frame and position in Earth frame.

Stability and performance properties of the proposed filters are derived, and the region of attraction is explicitly characterized. The intrinsic multirate characteristics of the available sensor suite is also addressed, and a synthesis methodology based on optimality results for periodic systems is presented. An algorithm to provide for attitude observations is proposed, that computes pitch and roll from the pendular measurements, and yaw using the magnetic field observations, thus referred as magneto-pendular sensor (MPS).

The navigation system structure is designed to be easily implemented in a low-cost, low-power consumption hardware architecture. The Euler angles are chosen as the state space representation for the rigid body attitude filter, due to its simplicity. Steady-state feedback gains are adopted in the filter design, and the structure of the resulting complementary filters can be described in block diagram form, allowing for straightforward implementation of the proposed architecture. Note that classical navigation systems, such as those based on the EKF algorithm, require online computation of the covariances and of the gains, which may allocate most of the few computational resources found in low-power low-performance hardware. The complementary filters proposed in this work are time-varying, however the adopted gains are constant and computed offline using an auxiliary time invariant design system. Consequently, a computationally inexpensive, steady-state like architecture is obtained, that is easy to implement and test in low-cost hardware, with stability and performance properties for the trimming trajectories of ASCs. The performance results of the navigation system are validated using experimental data obtained in tests at sea with the DELFIMx catamaran.

This paper is organized as follows. Section II presents the complementary filters for attitude and position estimation. Stability properties are derived and the conditions that guarantee performance are discussed. Section III focuses on the implementation of the attitude and position filters, that are combined to produce a navigation system with the multirate architecture, and details the MPS algorithm. The navigation system performance is shown in the experimental results of Section IV, for the DELFIMx catamaran sea trials. Concluding remarks and future work are pointed out in Section V.

II. ATTITUDE AND POSITION COMPLEMENTARY FILTERS

In this section, complementary filters for attitude and position estimation are proposed, and their stability and performance properties are derived. The design of the filters in the frequency

angle can be computed from the Earth's magnetic field measurements provided by a magnetometer triad. The choice of attitude observation depends on the available sensors and computational resources, and hence the attitude observation adopted in this work is detailed later in the navigation system implementation section. Consider the following auxiliary linear time invariant system:

$$\begin{bmatrix} \mathbf{x}_{\lambda k+1} \\ \mathbf{x}_{b k+1} \end{bmatrix} = \begin{bmatrix} \mathbf{I} & -T\mathbf{I} \\ \mathbf{0} & \mathbf{I} \end{bmatrix} \begin{bmatrix} \mathbf{x}_{\lambda k} \\ \mathbf{x}_{b k} \end{bmatrix} + \begin{bmatrix} -T\mathbf{I} & \mathbf{0} \\ \mathbf{0} & \mathbf{I} \end{bmatrix} \begin{bmatrix} \mathbf{w}_{\omega_r k} \\ \mathbf{w}_{b k} \end{bmatrix} \quad (6a)$$

$$\mathbf{y}_{x k} = [\mathbf{I} \quad \mathbf{0}] \begin{bmatrix} \mathbf{x}_{\lambda k} \\ \mathbf{x}_{b k} \end{bmatrix} + \mathbf{v}_{\lambda k} \quad (6b)$$

which will be used in the sequel as the frequency domain design setup for the time varying attitude filter (5). In the proposed design technique, the feedback gains $K_{1\lambda}$ and $K_{2\lambda}$ in (5) are identified with the steady-state Kalman gains for the system (6), where the covariance matrices Ξ_{ω} , Ξ_b , and Θ_{λ} act as ‘‘tuning knobs’’ to shape the desired frequency response of the attitude filter.

The time-invariant system (6) adopted for the determination of the feedback gains and associated frequency response is similar to the attitude kinematics (4) for $\mathbf{Q}(\bar{\boldsymbol{\lambda}}) = \mathbf{Q}(\mathbf{0})$. Although this suggests at first glance that the properties of the proposed filter could be limited to the specific case of $\bar{\boldsymbol{\lambda}}_k = \mathbf{0}$, the filter is in fact asymptotically stable for any attitude trajectory parameterized by nonsingular Euler angle configurations. The stability properties are derived in the following theorem for the specific case of Z - Y - X Euler angles, however the extension of the results to other Euler angle set conventions [30] is immediate.

Theorem 1: Consider the discrete-time attitude kinematics (4). Let $K_{1\lambda}$ and $K_{2\lambda}$ be the steady-state Kalman gains for the system (6) and assume that the pitch described by the platform is bounded, $|\bar{\theta}| \leq \theta_{\max} < \pi/2$. Then the attitude complementary filter (5) is uniformly asymptotically stable (UAS).

Proof: Let $\tilde{\boldsymbol{\lambda}}_k = \bar{\boldsymbol{\lambda}}_k - \hat{\boldsymbol{\lambda}}_k$, $\tilde{\mathbf{b}}_{\omega k} = \bar{\mathbf{b}}_{\omega k} - \hat{\mathbf{b}}_{\omega k}$ denote the estimation errors. The associated estimation error dynamics are given by

$$\begin{bmatrix} \tilde{\boldsymbol{\lambda}}_{k+1} \\ \tilde{\mathbf{b}}_{k+1} \end{bmatrix} = \begin{bmatrix} \mathbf{Q}(\bar{\boldsymbol{\lambda}}_k)(\mathbf{I} - K_{1\lambda})\mathbf{Q}^{-1}(\bar{\boldsymbol{\lambda}}_{k-1}) & -T\mathbf{Q}(\bar{\boldsymbol{\lambda}}_k) \\ -K_{2\lambda}\mathbf{Q}^{-1}(\bar{\boldsymbol{\lambda}}_{k-1}) & \mathbf{I} \end{bmatrix} \begin{bmatrix} \tilde{\boldsymbol{\lambda}}_k \\ \tilde{\mathbf{b}}_k \end{bmatrix} + \begin{bmatrix} -T\mathbf{Q}(\bar{\boldsymbol{\lambda}}_k) & \mathbf{0} \\ \mathbf{0} & \mathbf{I} \end{bmatrix} \begin{bmatrix} \mathbf{w}_{\omega_r k} \\ \mathbf{w}_{b k} \end{bmatrix} + \begin{bmatrix} \mathbf{Q}(\bar{\boldsymbol{\lambda}}_k)(\mathbf{I} - K_{1\lambda}) - \mathbf{Q}(\bar{\boldsymbol{\lambda}}_{k-1}) \\ -K_{2\lambda} \end{bmatrix} \mathbf{v}_{\lambda k}. \quad (7)$$

By definition, the filter is said to be UAS if the origin of the system (7) is UAS in the absence of state and measurement noises [33]. However, the state and measurement noises are denoted in the proof for the sake of convenience. The system (6) can be written in the compact state-space formulation

$$\mathbf{x}_{k+1} = \mathbf{F}\mathbf{x}_k + \mathbf{G}\mathbf{w}_k, \quad \mathbf{y}_k = \mathbf{H}\mathbf{x}_k + \mathbf{v}_k \quad (8)$$

where $\mathbf{x}_k = [\mathbf{x}'_{\lambda k} \quad \mathbf{x}'_{b k}]'$, $\mathbf{w}_k = [\mathbf{w}'_{\omega_r k} \quad \mathbf{w}'_{b k}]'$, $\mathbf{y}_k = \mathbf{y}_{x k}$, $\mathbf{v}_k = \mathbf{v}_{\lambda k}$, $\mathbf{F} = \begin{bmatrix} \mathbf{I} & -T\mathbf{I} \\ \mathbf{0} & \mathbf{I} \end{bmatrix}$, $\mathbf{G} = \begin{bmatrix} -T\mathbf{I} & \mathbf{0} \\ \mathbf{0} & \mathbf{I} \end{bmatrix}$, and $\mathbf{H} = [\mathbf{I} \quad \mathbf{0}]$. It is straightforward to show that $[\mathbf{F}, \mathbf{H}]$ is detectable

and $[\mathbf{F}, \mathbf{G}]$ is completely stabilizable, hence the closed-loop system

$$\tilde{\mathbf{x}}_{k+1} = (\mathbf{F} - \mathbf{K}\mathbf{H})\tilde{\mathbf{x}}_k + \mathbf{G}\mathbf{w}_k - \mathbf{K}\mathbf{v}_k \quad (9)$$

where $\mathbf{K} = [K'_{1\lambda} \quad K'_{2\lambda}]'$, is UAS [34]. Define the Lyapunov transformation of variables

$$\begin{bmatrix} \tilde{\boldsymbol{\lambda}}_{x k} \\ \tilde{\mathbf{b}}_{x k} \end{bmatrix} = \mathbf{T}_k \begin{bmatrix} \tilde{\boldsymbol{\lambda}}_{\lambda k} \\ \tilde{\mathbf{x}}_{b k} \end{bmatrix}, \quad \mathbf{T}_k = \begin{bmatrix} \mathbf{Q}(\bar{\boldsymbol{\lambda}}_{k-1}) & \mathbf{0} \\ \mathbf{0} & \mathbf{I} \end{bmatrix} \quad (10)$$

that is well defined [35] because $\bar{\theta}$ is bounded by assumption. Applying the transformation of variables \mathbf{T}_k to (9) yields

$$\begin{bmatrix} \tilde{\boldsymbol{\lambda}}_{x k+1} \\ \tilde{\mathbf{b}}_{x k+1} \end{bmatrix} = \mathbf{T}_{k+1}(\mathbf{F} - \mathbf{K}\mathbf{H})\mathbf{T}_k^{-1} \begin{bmatrix} \tilde{\boldsymbol{\lambda}}_{x k} \\ \tilde{\mathbf{b}}_{x k} \end{bmatrix} + \mathbf{T}_{k+1}\mathbf{G}\mathbf{w}_k - \mathbf{T}_{k+1}\mathbf{K}\mathbf{v}_k = \begin{bmatrix} \mathbf{Q}(\bar{\boldsymbol{\lambda}}_k)(\mathbf{I} - K_{1\lambda})\mathbf{Q}^{-1}(\bar{\boldsymbol{\lambda}}_{k-1}) & -T\mathbf{Q}(\bar{\boldsymbol{\lambda}}_k) \\ -K_{2\lambda}\mathbf{Q}^{-1}(\bar{\boldsymbol{\lambda}}_{k-1}) & \mathbf{I} \end{bmatrix} \times \begin{bmatrix} \tilde{\boldsymbol{\lambda}}_{x k} \\ \tilde{\mathbf{b}}_{x k} \end{bmatrix} + \begin{bmatrix} -T\mathbf{Q}(\bar{\boldsymbol{\lambda}}_k)\mathbf{w}_{\omega_r k} \\ \mathbf{w}_{b k} \end{bmatrix} - \begin{bmatrix} \mathbf{Q}(\bar{\boldsymbol{\lambda}}_k)K_{1\lambda} \\ K_{2\lambda} \end{bmatrix} \mathbf{v}_{\lambda k}. \quad (11)$$

The origin of (9) is UAS and, by the properties of Lyapunov transformations, the origin of (11) is UAS. Hence, the origin of (7) is uniform asymptotic stability, as desired. ■

The stability properties derived in Theorem 1 are valid for nonsingular configurations, where the pitch satisfies $\bar{\theta} < \pi/2$. This is a weak condition for most terrestrial and oceanic applications, namely those based on autonomous surface crafts, that are studied in this paper to illustrate the proposed navigation system. The stability results can be extended for time-varying Kalman gains, however the proposed complementary filter is designed in the frequency domain by means of the time-invariant formulation (6), to obtain a desired transfer function that merges the low-frequency contents of the attitude observations with the high-frequency information from the angular rate readings. Steady-state Kalman filter gains are adopted to yield an asymptotically stable filter that can be easily implemented and tested in low-cost hardware.

Interestingly enough, under operating conditions found in some terrestrial and oceanic applications, the gains adopted in the proposed filter (5) are identified with the steady-state gains of the Kalman filter for the system (4). This implies that, for ASC trimming maneuvers found in surveillance operations, the performance of the proposed attitude filter is identical to that of a Kalman filter designed for the time-varying system (4).

Theorem 2: Let the state and observation disturbances in the attitude kinematics (4) be characterized by the Gaussian white noises $\mathbf{w}_{\omega_r} \sim \mathcal{N}(\mathbf{0}, \Xi_{\omega})$, $\mathbf{w}_b \sim \mathcal{N}(\mathbf{0}, \Xi_b)$, and $\mathbf{v}_{\lambda} \sim \mathcal{N}(\mathbf{0}, \Theta_{\lambda})$, respectively, and assume that the pitch and roll angles are constant. Then the complementary attitude filter (5) is the ‘‘steady-state’’ Kalman filter for the system (4) in the sense that the Kalman feedback gain $K_{\text{opt } k}$ converges asymptotically as follows:

$$\lim_{k \rightarrow \infty} \left\| K_{\text{opt } k} - \begin{bmatrix} \mathbf{Q}(\bar{\boldsymbol{\lambda}}_k)(K_{1\lambda} - \mathbf{I}) + \mathbf{Q}(\bar{\boldsymbol{\lambda}}_{k-1}) \\ K_{2\lambda} \end{bmatrix} \right\| = 0. \quad (12)$$

Proof: The estimation error covariance matrix of the Kalman filter for the system (6) satisfies

$$\mathbf{P}_{x\lambda k+1|k} = \mathbf{F}\mathbf{P}_{x\lambda k|k-1}\mathbf{F}' + \mathbf{G}\Xi\mathbf{G}' - \mathbf{F}\mathbf{P}_{x\lambda k|k-1}\mathbf{H}'\mathbf{S}_{P\lambda k}^{-1}\mathbf{H}\mathbf{P}_{x\lambda k|k-1}\mathbf{F}' \quad (13)$$

where

$$\mathbf{S}_{P\lambda k} = \mathbf{H}\mathbf{P}_{x\lambda k|k-1}\mathbf{H}' + \Theta_\lambda, \quad \Xi = \begin{bmatrix} \Xi_\omega & \mathbf{0} \\ \mathbf{0} & \Xi_b \end{bmatrix}$$

see [33] and [34] for a derivation of (13). Given the transformation of variables (10), the covariance matrix

$$\Sigma_{x\lambda k+1|k} = E \left(\begin{bmatrix} \tilde{\lambda}_{x k+1} \\ \tilde{\mathbf{b}}_{x k+1} \end{bmatrix} \begin{bmatrix} \tilde{\lambda}'_{x k+1} & \tilde{\mathbf{b}}'_{x k+1} \end{bmatrix} \right)$$

is given by $\Sigma_{x\lambda k+1|k} = \mathbf{T}_{k+1}\mathbf{P}_{x\lambda k+1|k}\mathbf{T}'_{k+1}$ and, using (13), satisfies

$$\begin{aligned} & \mathbf{T}_{k+1}^{-1}\Sigma_{x\lambda k+1|k}\mathbf{T}'_{k+1} \\ &= \mathbf{F}\mathbf{T}_k^{-1}\Sigma_{x\lambda k|k-1}\mathbf{T}'_k\mathbf{F}' + \mathbf{G}\Xi\mathbf{G}' \\ & \quad - \mathbf{F}\mathbf{T}_k^{-1}\Sigma_{x\lambda k|k-1}\mathbf{T}'_k\mathbf{H}'\mathbf{S}_{P\lambda k}^{-1}\mathbf{H}\mathbf{T}_k^{-1}\Sigma_{x\lambda k|k-1}\mathbf{T}'_k\mathbf{F}' \\ & \Downarrow \\ & \Sigma_{x\lambda k+1|k} \\ &= \mathbf{T}_{k+1}\mathbf{F}\mathbf{T}_k^{-1}\Sigma_{x\lambda k|k-1}\mathbf{T}'_k\mathbf{F}'\mathbf{T}'_{k+1} \\ & \quad + \mathbf{T}_{k+1}\mathbf{G}\Xi\mathbf{G}'\mathbf{T}'_{k+1} - \mathbf{T}_{k+1}\mathbf{F}\mathbf{T}_k^{-1}\Sigma_{x\lambda k|k-1}\mathbf{T}'_k \\ & \quad \cdot \mathbf{H}'\mathbf{S}_{\Sigma\lambda k}^{-1}\mathbf{H}\mathbf{T}_k^{-1}\Sigma_{x\lambda k|k-1}\mathbf{T}'_k\mathbf{F}'\mathbf{T}'_{k+1} \end{aligned}$$

where $\mathbf{S}_{\Sigma\lambda k} = \mathbf{H}\mathbf{T}_k^{-1}\Sigma_{x\lambda k|k-1}\mathbf{T}'_k\mathbf{H}' + \Theta_\lambda$.

With a slight abuse of notation, let $K_{1\lambda k}$ and $K_{2\lambda k}$ denote the time-varying Kalman gains for the system (6) and formulate the attitude filter (5) with time-varying gains

$$\begin{bmatrix} \hat{\lambda}_{k+1} \\ \hat{\mathbf{b}}_{k+1} \end{bmatrix} = \begin{bmatrix} \mathbf{I} & -T\mathbf{Q}(\bar{\lambda}_k) \\ \mathbf{0} & \mathbf{I} \end{bmatrix} \begin{bmatrix} \hat{\lambda}_k \\ \hat{\mathbf{b}}_k \end{bmatrix} + \begin{bmatrix} T\mathbf{Q}(\bar{\lambda}_k) \\ \mathbf{0} \end{bmatrix} \boldsymbol{\omega}_{r k} \\ + \begin{bmatrix} \mathbf{Q}(\bar{\lambda}_k)(K_{1\lambda k} - \mathbf{I}) + \mathbf{Q}(\bar{\lambda}_{k-1}) \\ K_{2\lambda k} \end{bmatrix} (\mathbf{y}_{\lambda k} - \hat{\mathbf{y}}_{\lambda k}). \quad (14)$$

To identify the attitude filter (5) as the steady-state Kalman filter for the system (4), it is shown that the attitude filter (14) is the Kalman filter for the system (4). This condition is satisfied if: 1) $\Sigma_{x\lambda k+1|k}$ is the error covariance of the attitude filter (14) and that 2) $\Sigma_{x\lambda k+1|k}$ is the error covariance of the optimal (i.e., Kalman) filter for the attitude kinematics (4), for a discussion on the optimality of the Kalman filter and uniqueness of the optimal gains, the reader is referred to [33], [34].

The condition of constant pitch and roll implies that $\mathbf{Q}(\bar{\lambda}_{k+1}) = \mathbf{Q}(\bar{\lambda}_k)$, hence the kinematics (7) and (11) are identical, $[\tilde{\lambda}'_{x k} \ \tilde{\mathbf{b}}'_{x k}]' = [\tilde{\lambda}'_{x k} \ \tilde{\mathbf{b}}'_{x k}]'$ and $\Sigma_{x\lambda k+1|k}$ is the error covariance matrix of the attitude filter (14).

The matrix $\Sigma_{x\lambda k+1|k}$ is the covariance error of the Kalman filter for the system

$$\mathbf{z}_{k+1} = \mathbf{T}_{k+1}\mathbf{F}\mathbf{T}_k^{-1}\mathbf{z}_k + \mathbf{T}_{k+1}\mathbf{G}\mathbf{w}_{z k} \quad (15a)$$

$$\mathbf{y}_{z k} = \mathbf{H}\mathbf{T}_k^{-1}\mathbf{z}_k + \mathbf{v}_{z k} \quad (15b)$$

where $\mathbf{z}_k \in \mathbb{R}^6$, $\mathbf{w}_z \sim \mathcal{N}(\mathbf{0}, \Xi)$, $\mathbf{v}_z \sim \mathcal{N}(\mathbf{0}, \Theta_\lambda)$. Using $\mathbf{Q}(\bar{\lambda}_{k+1}) = \mathbf{Q}(\bar{\lambda}_k)$, the matrices of the system (15) are given by

$$\begin{aligned} \mathbf{T}_{k+1}\mathbf{F}\mathbf{T}_k^{-1} &= \begin{bmatrix} \mathbf{I} & -T\mathbf{Q}(\bar{\lambda}_k) \\ \mathbf{0} & \mathbf{I} \end{bmatrix} \\ \mathbf{T}_{k+1}\mathbf{G} &= \begin{bmatrix} -T\mathbf{Q}(\bar{\lambda}_k) & \mathbf{0} \\ \mathbf{0} & \mathbf{I} \end{bmatrix} \\ \mathbf{H}\mathbf{T}_k^{-1} &= [\mathbf{Q}^{-1}(\bar{\lambda}_{k-1}) \ \mathbf{0}] \end{aligned}$$

which are identical to the state matrices of the attitude kinematics (4) with attitude observation given by (5b). Consequently, the attitude filter (14) produces the optimal estimation error covariance matrix $\Sigma_{x\lambda k+1|k}$ for the system (4) and, by uniqueness, the attitude filter (14) is a Kalman filter. Using $K_{1\lambda k} \rightarrow K_{1\lambda}$ and $K_{2\lambda k} \rightarrow K_{2\lambda}$ as $k \rightarrow \infty$ yields (12), that completes the proof. ■

The performance results presented in Theorem 2 hold for applications where the pitch and roll angles are constant or can be considered approximately constant. It should be emphasized that it is of interest for terrestrial and oceanic platforms considered in this work, subject to repetitive monitoring trajectories. For the case of time-varying pitch and roll angles, and for aggressive maneuvers, the performance of the complementary and of the Kalman filters can be compared offline by computing the estimation error covariances of the filters, as detailed in Appendix A.

In spite of the performance results presented in Theorem 2, the design of the feedback gains is performed in the frequency domain due to the characteristics of the attitude aiding sensor at hand, and to unmodeled sensor disturbances often found in experimental setups. This approach exploits the low-frequency region where the attitude observations are typically more accurate, and the high-frequency region where the integration of the rate gyro yields better attitude measurements.

Also, the attitude and position filters are derived independently, which allows for the separate tuning of the filters, and the use of the attitude filter as standalone algorithm in applications where only attitude estimation is required. Due to the independent design of the filters, the cross-correlation between acceleration and attitude is ignored, however its contribution to attitude estimation is usually negligible in the considered oceanic applications. To see this, the cross-correlation can be analyzed using a perturbational analysis [3], and can be modeled as

$$\frac{d^E \hat{\mathbf{v}} - E \bar{\mathbf{v}}}{dt} \approx -E \mathbf{a}_r \times \delta\boldsymbol{\phi} + \bar{\mathbf{R}}\mathbf{w}_{a_r}$$

where $\delta\boldsymbol{\phi}$ is the Euler angle-axis parametrization of the rotation error matrix given by $\bar{\mathbf{R}} = \bar{\mathbf{R}}\bar{\mathbf{R}}'$, $E\mathbf{a}_r$ is the accelerometer reading expressed in Earth coordinates, and \mathbf{w}_{a_r} is the accelerometer measurement noise. In many applications, the measurement \mathbf{a}_r is dominated by the gravitational acceleration, i.e., $E\mathbf{a}_r \approx [a_x \ a_y \ g]'$ with $a_x \ll g$ and $a_y \ll g$. Therefore, \mathbf{a}_r will contribute mostly to the observability of the x and y components of $\delta\boldsymbol{\phi}$, which are not critical for ASCs. Later in this work, the performance of the complementary filter is studied for the experimental data obtained on-board the DELFIMx catamaran.

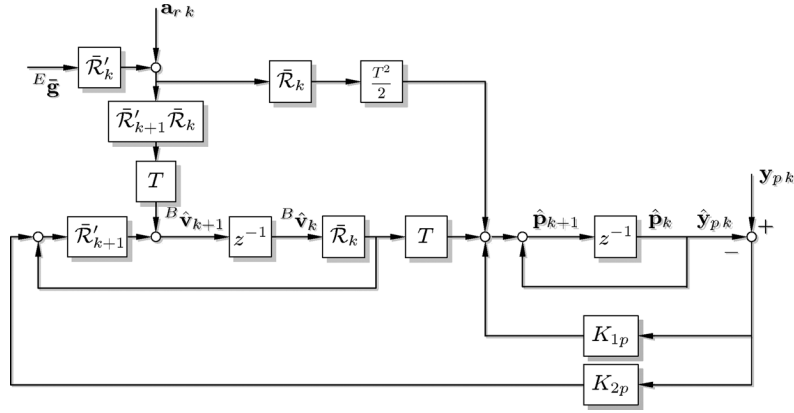


Fig. 4. Position complementary filter.

B. Position Filter

The continuous-time position kinematics are given by

$$\dot{\mathbf{p}} = \bar{\mathbf{v}}, \quad \dot{\bar{\mathbf{v}}} = \bar{\mathcal{R}}^B \bar{\mathbf{a}}$$

where $\bar{\mathbf{p}}$ and $\bar{\mathbf{v}}$ are the position and velocity in Earth frame coordinates, $\bar{\mathcal{R}}$ is the shorthand notation for the rotation matrix from body frame $\{B\}$ to Earth frame $\{E\}$ coordinates, and ${}^B \bar{\mathbf{a}}$ is the acceleration in body frame coordinates. The discrete-time equivalent is obtained by sample-and-hold of the inputs [32] and is given by

$$\bar{\mathbf{p}}_{k+1} = \bar{\mathbf{p}}_k + T \bar{\mathbf{v}}_k + \frac{T^2}{2} \bar{\mathcal{R}}_k \bar{\mathbf{a}}_k, \quad \bar{\mathbf{v}}_{k+1} = \bar{\mathbf{v}}_k + T \bar{\mathcal{R}}_k {}^B \bar{\mathbf{a}}_k. \quad (16)$$

The accelerometer measures the specific force, which is the difference between the inertial and the gravitational accelerations of the rigid body [3], ${}^B \bar{\mathbf{a}}_k$ and ${}^B \bar{\mathbf{g}}_k$, respectively, expressed in body frame coordinates

$$\mathbf{a}_{r,k} = {}^B \bar{\mathbf{a}}_k - {}^B \bar{\mathbf{g}}_k + \mathbf{w}_{a_r}$$

where $\mathbf{w}_{a_r} \sim \mathcal{N}(\mathbf{0}, \Xi_a)$ is zero-mean, Gaussian white noise. The position kinematics (16) using the accelerometer measurements are described by

$$\begin{bmatrix} \bar{\mathbf{p}}_{k+1} \\ {}^B \bar{\mathbf{v}}_{k+1} \end{bmatrix} = \begin{bmatrix} \mathbf{I} & T \bar{\mathcal{R}}_k \\ \mathbf{0} & \bar{\mathcal{R}}'_{k+1} \bar{\mathcal{R}}_k \end{bmatrix} \begin{bmatrix} \bar{\mathbf{p}}_k \\ {}^B \bar{\mathbf{v}}_k \end{bmatrix} + \begin{bmatrix} \frac{T^2}{2} \bar{\mathcal{R}}_k \\ T \bar{\mathcal{R}}'_{k+1} \bar{\mathcal{R}}_k \end{bmatrix} \cdot (\mathbf{a}_{r,k} + \bar{\mathcal{R}}'_k {}^E \bar{\mathbf{g}}) + \begin{bmatrix} \mathbf{I} & -\frac{T^2}{2} \bar{\mathcal{R}}_k \\ \mathbf{0} & -T \bar{\mathcal{R}}'_{k+1} \bar{\mathcal{R}}_k \end{bmatrix} \begin{bmatrix} \mathbf{w}_{p,k} \\ \mathbf{w}_{a_r,k} \end{bmatrix} \quad (17)$$

where ${}^B \bar{\mathbf{v}}_k = \bar{\mathcal{R}}'_k \bar{\mathbf{v}}_{k+1}$ is the velocity expressed in body coordinates, ${}^E \bar{\mathbf{g}}$ is the gravitational acceleration expressed in Earth coordinates, and $\mathbf{w}_p \sim \mathcal{N}(\mathbf{0}, \Xi_p)$ is zero-mean, Gaussian white noise that accounts for small disturbances in the position. The position observer kinematics, depicted in Fig. 4, are given by

$$\begin{bmatrix} \hat{\mathbf{p}}_{k+1} \\ {}^B \hat{\mathbf{v}}_{k+1} \end{bmatrix} = \begin{bmatrix} \mathbf{I} & T \bar{\mathcal{R}}_k \\ \mathbf{0} & \bar{\mathcal{R}}'_{k+1} \bar{\mathcal{R}}_k \end{bmatrix} \begin{bmatrix} \hat{\mathbf{p}}_k \\ {}^B \hat{\mathbf{v}}_k \end{bmatrix} + \begin{bmatrix} \frac{T^2}{2} \bar{\mathcal{R}}_k \\ T \bar{\mathcal{R}}'_{k+1} \bar{\mathcal{R}}_k \end{bmatrix} (\mathbf{a}_{r,k} + \bar{\mathcal{R}}'_k {}^E \bar{\mathbf{g}}) + \begin{bmatrix} K_{1p} \\ \bar{\mathcal{R}}'_{k+1} K_{2p} \end{bmatrix} (\mathbf{y}_{p,k} - \hat{\mathbf{y}}_{p,k}) \quad (18a)$$

$$\hat{\mathbf{y}}_{p,k} = \hat{\mathbf{p}}_k, \quad \mathbf{y}_{p,k} = \bar{\mathbf{p}}_k + \mathbf{v}_{p,k} \quad (18b)$$

where $\mathbf{y}_{p,k}$ is the position computed using the readings of the GPS receiver, and $\mathbf{v}_p \sim \mathcal{N}(\mathbf{0}, \Theta_p)$ is zero-mean, Gaussian observation noise. The propulsion force of a vehicle is, in general, physically oriented along a body fixed axis, producing a predominant body fixed direction of motion, e.g., when thrusters are mounted and act along the x -axis of the body, the main velocity variations are naturally expressed along that axis. Also, high angular rates due to aggressive maneuvering introduce high-frequency shifts in Earth frame velocity, while the velocity in the body frame remains aligned with the vehicle's predominant direction of motion, e.g., the body velocity of a ship remains constant while describing uniform circular motion but the components of the velocity vector in Earth coordinates are sinusoidal. Consequently, the velocity estimate of the position filter is expressed in body frame coordinates, as opposed to being expressed in Earth frame, to reduce bandwidth requirements under attitude changes and vehicle actuation.

The feedback terms K_{1p} and K_{2p} are identified with the Kalman filter gains for the system

$$\begin{bmatrix} \mathbf{x}_{p,k+1} \\ \mathbf{x}_{v,k+1} \end{bmatrix} = \begin{bmatrix} \mathbf{I} & T \mathbf{I} \\ \mathbf{0} & \mathbf{I} \end{bmatrix} \begin{bmatrix} \mathbf{x}_{p,k} \\ \mathbf{x}_{v,k} \end{bmatrix} + \begin{bmatrix} \mathbf{I} & -\frac{T^2}{2} \\ \mathbf{0} & -T \end{bmatrix} \begin{bmatrix} \mathbf{w}_{p,k} \\ \mathbf{w}_{v,k} \end{bmatrix} \quad (19a)$$

$$\mathbf{y}_{x,k} = \begin{bmatrix} \mathbf{I} & \mathbf{0} \end{bmatrix} \begin{bmatrix} \mathbf{x}_{p,k} \\ \mathbf{x}_{v,k} \end{bmatrix} + \mathbf{v}_{p,k} \quad (19b)$$

where $\mathbf{w}_v \sim \mathcal{N}(\mathbf{0}, \Xi_a)$ is zero-mean, Gaussian white noise with the covariance of the accelerometer noise \mathbf{w}_{a_r} .

In the design of the position filter, the covariance matrices Ξ_p , Ξ_a , and Θ_p are used as tuning knobs to shape the frequency response of the filter. Accelerometer bias is compensated offline, since the limited dynamics of surface crafts are usually insufficient for online triaxial accelerometer bias estimation, more details on the observability analysis and online calibration maneuvers for GPS/INS systems can be found in [36], [37]. The offline calibration of the accelerometer bias was found suitable for the duration of the DELFIMx catamaran missions, as shown in the experimental validation presented later in this work.

The stability and performance of the position complementary filter (18), using the steady-state gains obtained for the system (19), are addressed in the following theorems.

Theorem 3: Consider the discrete-time position kinematics (17), and let K_{1p} and K_{2p} be the steady-state Kalman filter gains for the system (19). Then the position complementary filter (18) is UAS.

Proof: The structure of the proof is similar to that of Theorem 1. Define the estimation errors $\tilde{\mathbf{p}}_k = \bar{\mathbf{p}}_k - \hat{\mathbf{p}}_k$ and ${}^B\tilde{\mathbf{v}}_k = {}^B\bar{\mathbf{v}}_k - {}^B\hat{\mathbf{v}}_k$. The associated kinematics are described by

$$\begin{bmatrix} \tilde{\mathbf{p}}_{k+1} \\ {}^B\tilde{\mathbf{v}}_{k+1} \end{bmatrix} = \begin{bmatrix} \mathbf{I} - K_{1p} & T\bar{\mathcal{R}}_k \\ -K_{2p} & \bar{\mathcal{R}}'_{k+1}\bar{\mathcal{R}}_k \end{bmatrix} \begin{bmatrix} \tilde{\mathbf{p}}_k \\ {}^B\tilde{\mathbf{v}}_k \end{bmatrix} + \begin{bmatrix} \mathbf{I} & -\frac{T^2}{2}\bar{\mathcal{R}}_k \\ \mathbf{0} & -T\bar{\mathcal{R}}'_{k+1}\bar{\mathcal{R}}_k \end{bmatrix} \begin{bmatrix} \mathbf{w}_{pk} \\ \mathbf{w}_{a_r k} \end{bmatrix} - \begin{bmatrix} K_{1p} \\ \bar{\mathcal{R}}'_{k+1}K_{2p} \end{bmatrix} \mathbf{v}_{pk}. \quad (20)$$

The compact state space formulation for the system (19) is given by

$$\mathbf{x}_{k+1} = \mathbf{F}\mathbf{x}_k + \mathbf{G}\mathbf{w}_k, \quad \mathbf{y}_k = \mathbf{H}\mathbf{x}_k + \mathbf{v}_k \quad (21)$$

where $\mathbf{x}_k = [\mathbf{x}'_{pk} \quad \mathbf{x}'_{vk}]'$, $\mathbf{w}_k = [\mathbf{w}'_{pk} \quad \mathbf{w}'_{vk}]'$, $\mathbf{y}_k = \mathbf{y}_{xk}$, $\mathbf{v}_k = \mathbf{v}_{pk}$

$$\mathbf{F} = \begin{bmatrix} \mathbf{I} & T\mathbf{I} \\ \mathbf{0} & \mathbf{I} \end{bmatrix}, \quad \mathbf{G} = \begin{bmatrix} \mathbf{I} & -T^2/2 \\ \mathbf{0} & -T \end{bmatrix}$$

and $\mathbf{H} = [\mathbf{I} \quad \mathbf{0}]$. The pairs $[\mathbf{F}, \mathbf{H}']$ and $[\mathbf{F}, \mathbf{G}]$ are detectable and completely stabilizable, respectively and the closed-loop system

$$\tilde{\mathbf{x}}_{k+1} = (\mathbf{F} - \mathbf{K}\mathbf{H})\tilde{\mathbf{x}}_k + \mathbf{G}\mathbf{w}_k - \mathbf{K}\mathbf{v}_k \quad (22)$$

where $\mathbf{K} = [K'_{1p} \quad K'_{2p}]'$, is UAS [34]. Define the Lyapunov transformation of variables, adopted in previous work by the authors [38], given by

$$\begin{bmatrix} \tilde{\mathbf{p}}_k \\ \tilde{\mathbf{v}}_k \end{bmatrix} = \mathbf{T}_k \begin{bmatrix} \tilde{\mathbf{x}}_{pk} \\ \tilde{\mathbf{x}}_{vk} \end{bmatrix}, \quad \mathbf{T}_k = \begin{bmatrix} \mathbf{I} & \mathbf{0} \\ \mathbf{0} & \bar{\mathcal{R}}_k \end{bmatrix} \quad (23)$$

and consider $\mathbf{w}_{vk} = \bar{\mathcal{R}}_k \mathbf{w}_{a_r k}$. Applying the Lyapunov transformation to (22) yields (20), and hence the origin of (20) is uniformly asymptotically stable by the properties of Lyapunov transformations [35]. ■

In the following theorem it is shown that the proposed position filter is identified with the steady-state Kalman filter for the position kinematics (18), under the mild assumption that the Gaussian white noises of the accelerometer triad are stochastically independent and characterized by the same variance. The stochastic independence is verified in realistic setups where the acceleration measurements are provided by three sensors from the same model, mounted orthogonally.

Theorem 4: Let the state and observation disturbances in the position kinematics (17) be characterized by Gaussian white noises $\mathbf{w}_p \sim \mathcal{N}(\mathbf{0}, \Xi_p)$, $\mathbf{w}_{a_r} \sim \mathcal{N}(\mathbf{0}, \xi_a \mathbf{I})$, and $\mathbf{v}_p \sim \mathcal{N}(\mathbf{0}, \Theta_p)$. Then the position complementary filter (18) is the ‘‘steady-state’’ Kalman filter for the system (17) in the sense that the Kalman feedback gain $K_{\text{opt } k}$ converges asymptotically as follows:

$$\lim_{k \rightarrow \infty} \left\| K_{\text{opt } k} - \begin{bmatrix} K_{1p} \\ \bar{\mathcal{R}}'_{k+1}K_{2p} \end{bmatrix} \right\| = 0. \quad (24)$$

Proof: The estimation error covariance matrix of the Kalman filter for the system (21) satisfies

$$\begin{aligned} \mathbf{P}_{xp k+1|k} &= \mathbf{F}\mathbf{P}_{xp k|k-1}\mathbf{F}' + \mathbf{G}\Xi\mathbf{G}' \\ &\quad - \mathbf{F}\mathbf{P}_{xp k|k-1}\mathbf{H}'\mathbf{S}_{Pp}^{-1}\mathbf{H}\mathbf{P}_{xp k|k-1}\mathbf{F}' \end{aligned} \quad (25)$$

where

$$\mathbf{S}_{Pp} = \mathbf{H}\mathbf{P}_{xp k|k-1}\mathbf{H}' + \Theta, \quad \Xi = \begin{bmatrix} \Xi_p & \mathbf{0} \\ \mathbf{0} & \Xi_a \end{bmatrix}.$$

With a slight abuse of notation, let K_{1pk} and K_{2pk} denote the time-varying Kalman gains for the system (19) and formulate the attitude filter (18) with time-varying gains

$$\begin{bmatrix} \hat{\mathbf{p}}_{k+1} \\ {}^B\hat{\mathbf{v}}_{k+1} \end{bmatrix} = \begin{bmatrix} \mathbf{I} & T\bar{\mathcal{R}}_k \\ \mathbf{0} & \bar{\mathcal{R}}'_{k+1}\bar{\mathcal{R}}_k \end{bmatrix} \begin{bmatrix} \hat{\mathbf{p}}_k \\ {}^B\hat{\mathbf{v}}_k \end{bmatrix} + \begin{bmatrix} \frac{T^2}{2}\bar{\mathcal{R}}_k \\ T\bar{\mathcal{R}}'_{k+1}\bar{\mathcal{R}}_k \end{bmatrix} \cdot (\mathbf{a}_r + \bar{\mathcal{R}}_k{}^E\bar{\mathbf{g}}) + \begin{bmatrix} K_{1pk} \\ \bar{\mathcal{R}}'_{k+1}K_{2pk} \end{bmatrix} (\mathbf{y}_{pk} - \hat{\mathbf{y}}_{pk}). \quad (26)$$

Applying the Lyapunov transformation (23), the covariance matrix

$$\Sigma_{pk+1|k} = E \left(\begin{bmatrix} \tilde{\mathbf{p}}_{k+1} \\ \tilde{\mathbf{v}}_{k+1} \end{bmatrix} \begin{bmatrix} \tilde{\mathbf{p}}_{k+1} & \tilde{\mathbf{v}}'_{k+1} \end{bmatrix} \right)$$

is given by $\Sigma_{pk+1|k} = \mathbf{T}_{k+1}\mathbf{P}_{xk+1|k}\mathbf{T}'_{k+1}$ and satisfies

$$\begin{aligned} \Sigma_{pk+1|k} &= \mathbf{T}_{k+1}\mathbf{F}\mathbf{T}_k^{-1}\Sigma_{pk|k-1}\mathbf{T}_k^{-1}\mathbf{F}'\mathbf{T}'_{k+1} \\ &\quad + \mathbf{T}_{k+1}\mathbf{G}\Xi\mathbf{G}'\mathbf{T}'_{k+1} - \mathbf{T}_{k+1}\mathbf{F}\mathbf{T}_k^{-1}\Sigma_{pk|k-1}\mathbf{T}_k^{-1} \\ &\quad \cdot \mathbf{H}'\mathbf{S}_{\Sigma p k}^{-1}\mathbf{H}\mathbf{T}_k^{-1}\Sigma_{pk|k-1}\mathbf{T}_k^{-1}\mathbf{F}'\mathbf{T}'_{k+1} \end{aligned} \quad (27)$$

where $\mathbf{S}_{\Sigma p k} = \mathbf{H}\mathbf{T}_k^{-1}\Sigma_{pk|k-1}\mathbf{T}_k^{-1}\mathbf{H}' + \Theta$. Assuming that the accelerometer noise covariance matrix is diagonal, $\Xi_a = \xi_a \mathbf{I}$, the matrices in (27) are given by

$$\begin{aligned} \mathbf{T}_{k+1}\mathbf{F}\mathbf{T}_k^{-1} &= \begin{bmatrix} \mathbf{I} & T\bar{\mathcal{R}}_k \\ \mathbf{0} & \bar{\mathcal{R}}'_{k+1}\bar{\mathcal{R}}_k \end{bmatrix}, \quad \mathbf{H}\mathbf{T}_k^{-1} = [\mathbf{I} \quad \mathbf{0}] \\ \mathbf{T}_{k+1}\mathbf{G}\Xi\mathbf{G}'\mathbf{T}'_{k+1} &= \mathbf{T}_{k+1}\mathbf{G} \begin{bmatrix} \Xi_p & \mathbf{0} \\ \mathbf{0} & \Xi_a \end{bmatrix} \mathbf{G}'\mathbf{T}'_{k+1} \\ &= \mathbf{T}_{k+1}\mathbf{G} \begin{bmatrix} \Xi_p & \mathbf{0} \\ \mathbf{0} & \bar{\mathcal{R}}_k\Xi_a\bar{\mathcal{R}}'_k \end{bmatrix} \mathbf{G}'\mathbf{T}'_{k+1} \\ &= \begin{bmatrix} \mathbf{I} & -\frac{T^2}{2}\bar{\mathcal{R}}_k \\ \mathbf{0} & -T\bar{\mathcal{R}}'_{k+1}\bar{\mathcal{R}}_k \end{bmatrix} \begin{bmatrix} \Xi_p & \mathbf{0} \\ \mathbf{0} & \Xi_a \end{bmatrix} \\ &\quad \cdot \begin{bmatrix} \mathbf{I} & -\frac{T^2}{2}\bar{\mathcal{R}}_k \\ \mathbf{0} & -T\bar{\mathcal{R}}'_{k+1}\bar{\mathcal{R}}_k \end{bmatrix}' \end{aligned}$$

which shows that $\Sigma_{pk+1|k}$ is the optimal error covariance matrix for the position kinematics (17). Using $K_{1pk} \rightarrow K_{1p}$ and $K_{2pk} \rightarrow K_{2p}$ as $k \rightarrow \infty$ produces (24) and completes the proof. ■

Although some performance results are presented for the position filter, the closed-loop system is obtained by design in the frequency domain, and the feedback gains K_{1p} and K_{2p} are the steady-state Kalman gains for the design system (19). In this framework, the high-frequency contents of the accelerometer measurements are exploited, filtering out gravity and bias compensation errors, and merged with the low-frequency information available from the GPS position observations.

III. NAVIGATION SYSTEM IMPLEMENTATION

This section presents the overall navigation system architecture that builds on the attitude and position complementary filters derived separately in Section II, and discusses the problem of implementing the filter with different sampling rates.

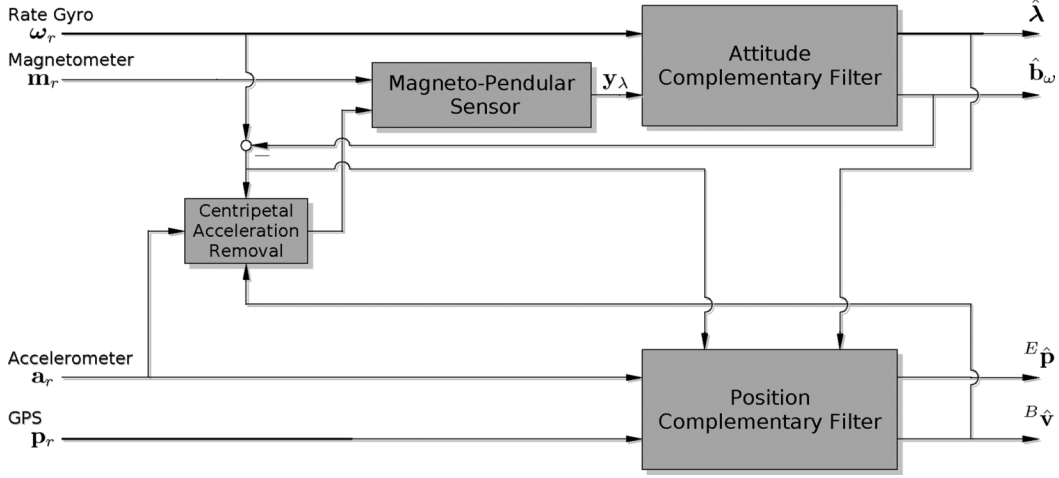


Fig. 5. Navigation system architecture.

A. Magneto-Pendular Sensor

The attitude observation $y_{\lambda k}$ in Euler angles coordinates is determined using the body and Earth frame representations of two vectors, namely the Earth's magnetic and gravitational fields. The problem of determining attitude using vector measurements is known in the literature as the orthogonal Procrustes problem [39] or as Wahba's problem [40] and several solutions have been proposed along time-spread articles [4]. The solution proposed in this work computes the Euler angles observation using a deterministic approach, similar to that of a TRIAD algorithm [41], [42]. Note that $y_{\lambda k}$ can be obtained using other attitude reconstruction algorithms and sensors, for more details see [4] and references therein.

The magnetic field vector is measured in the body frame by the magnetometer

$$\mathbf{m}_r = \mathbf{R}'_X(\bar{\phi})\mathbf{R}'_Y(\bar{\theta})\mathbf{R}'_Z(\bar{\psi})^E\bar{\mathbf{m}} + \mathbf{n}_m \quad (28)$$

where the magnetic field in Earth frame coordinates, denoted by ${}^E\bar{\mathbf{m}}$, is known, \mathbf{n}_m is the magnetometer measurement noise and $\mathbf{R}_X(\bar{\phi})$, $\mathbf{R}_Y(\bar{\theta})$, and $\mathbf{R}_Z(\bar{\psi})$ represent the roll, pitch, and yaw elementary rotation matrices, respectively. Denoting the projection of the magnetometer reading on the x - y plane by ${}^P\mathbf{m} = \mathbf{R}_Y(\bar{\theta})\mathbf{R}_X(\bar{\phi})\mathbf{m}_r$, the yaw angle is obtained by algebraic manipulation of (28), producing

$$\bar{\psi} = \arctan 2 \left({}^E\bar{m}_y {}^P m_x - {}^E\bar{m}_x {}^P m_y, {}^E\bar{m}_x {}^P m_x + {}^E\bar{m}_y {}^P m_y \right) \quad (29)$$

where the four quadrant arctan, denoted as $\arctan 2$, was adopted. The pitch and roll angles are obtained from the accelerometer, which is regarded as a pendular sensor

$$\mathbf{a}_p \approx -{}^B\bar{\mathbf{g}} = -\mathbf{R}'_X(\bar{\phi})\mathbf{R}'_Y(\bar{\theta})^E\bar{\mathbf{g}} = \begin{bmatrix} \bar{g} \sin \bar{\theta} \\ -\bar{g} \cos \bar{\theta} \sin \bar{\phi} \\ -\bar{g} \cos \bar{\theta} \cos \bar{\phi} \end{bmatrix} \quad (30)$$

where \mathbf{a}_p denotes the accelerometer reading assuming that external accelerations are negligible, ${}^E\bar{\mathbf{g}} = [0 \ 0 \ \bar{g}]'$ is the gravity vector in Earth frame coordinates, and \bar{g} is the local

gravitational acceleration. The pitch and roll angles are given by algebraic manipulation of (30), producing

$$\begin{aligned} \bar{\phi} &= \arctan 2(-a_y, -a_z) \\ \bar{\theta} &= \begin{cases} \arctan \left(\frac{-a_x \sin \bar{\phi}}{a_y} \right), & \sin \bar{\phi} \neq 0 \\ \arctan \left(\frac{-a_x \cos \bar{\phi}}{a_z} \right), & \cos \bar{\phi} \neq 0 \end{cases} \end{aligned} \quad (31)$$

that are independent of the magnitude of ${}^E\bar{\mathbf{g}}$ and hence do not require a model of the local gravitational acceleration \bar{g} .

The computation of pitch and roll angles using directly the accelerometer reading in (31) is distorted in the presence of external linear and angular accelerations. The accelerometer measurement model is given by [3]

$$\mathbf{a}_r = \frac{d {}^B\bar{\mathbf{v}}}{dt} + \bar{\boldsymbol{\omega}} \times {}^B\bar{\mathbf{v}} - {}^B\bar{\mathbf{g}} \quad (32)$$

where $d {}^B\bar{\mathbf{v}}/dt$ is the linear acceleration and $\bar{\boldsymbol{\omega}} \times {}^B\bar{\mathbf{v}}$ is the centripetal acceleration. Typical maneuvers of autonomous vehicles involve mostly short term linear accelerations, which hence are high-frequency and the resulting distortion in pitch and roll can be smoothed out by the complementary lowpass filter. On the other hand, centripetal accelerations occur even in trimming maneuvers, e.g., a helicoidal path, and must be compensated for. As depicted in Fig. 5, the pendular reading estimate $\hat{\mathbf{a}}_p$ used in (31) is obtained by compensating the centripetal acceleration

$$\hat{\mathbf{a}}_p = \mathbf{a}_r - \hat{\boldsymbol{\omega}} \times {}^B\hat{\mathbf{v}} \quad (33)$$

where $\hat{\boldsymbol{\omega}} = \boldsymbol{\omega}_r - \hat{\mathbf{b}}_{\omega}$ is the angular rate drawn from the rate gyro measurement with bias compensation and ${}^B\hat{\mathbf{v}}$ is the velocity estimate provided by the complementary position filter or by a Doppler sensor if available. The effect of linear acceleration in $\hat{\mathbf{a}}_p$ is compensated in the frequency domain by appropriate design of the complementary filter.

The yaw, pitch, and roll observations (29), (31), (33) define a virtual attitude sensor measurement that is referred to as magneto-pendular sensor (MPS). The MPS observation noise \mathbf{v}_{λ} is a nonlinear function of the magnetometer and accelerometer noises, the attitude of the vehicle and the (linear and angular)

acceleration compensation errors, and is mostly high-frequency due to the influence of linear accelerations. If modeled stochastically, the noise covariance Θ_λ can be inflated to account for the time-varying covariance of \mathbf{v}_λ , however this technique leads to undesirable performance degradation, for a discussion on the subject see [34] and references therein. In the frequency domain design approach, adopted in this work, the observation noise weight matrix is tuned to yield good steady-state high-frequency rejection of the MPS noise.

B. Complementary Filter Coupling

The proposed navigation system integrates the attitude and position complementary filters to produce an estimate of the vehicle attitude and position. The blocks of the diagram depicted in Fig. 5 have been introduced previously in this work: the attitude and position complementary filters are detailed in Section II and illustrated in Figs. 3 and 4, respectively, and the MPS and the centripetal acceleration removal blocks are detailed in Section III-A. The attitude terms in the position filter kinematics and the use of pendular readings to obtain the MPS measurement produce a coupling between the attitude and the position filters, illustrated by the block connections of Fig. 5, which are described as follows.

The attitude rotation matrix $\bar{\mathcal{R}}_k$ and the attitude update term $\bar{\mathcal{R}}'_{k+1}\bar{\mathcal{R}}_k$ are adopted in the kinematics of the position filter (18), as illustrated in the block diagram of Fig. 4. The attitude term $\bar{\mathcal{R}}_k$ is computed using the attitude filter estimate $\hat{\boldsymbol{\lambda}}_k$, which is the best attitude estimate available in the practical implementation of the navigation system, and the update term described by $\bar{\mathcal{R}}'_{k+1}\bar{\mathcal{R}}_k \approx e^{-T(\boldsymbol{\omega}_r k - \hat{\mathbf{b}}_{\omega k})_\times}$ is obtained using the rate gyro measurement and the bias estimate, where $(\mathbf{a})_\times$ is the skew symmetric matrix defined by the vector $\mathbf{a} \in \mathbb{R}^3$ such that $(\mathbf{a})_\times \mathbf{b} = \mathbf{a} \times \mathbf{b}$, $\mathbf{b} \in \mathbb{R}^3$. Likewise, the transformation matrix $\mathbf{Q}(\hat{\boldsymbol{\lambda}}_k)$ is constructed using the estimate $\hat{\boldsymbol{\lambda}}_k$ given by the attitude filter, that is the best attitude estimate available. The gravitational measurements used in the computation of the attitude measurement \mathbf{y}_λ are distorted by linear and angular accelerations. As a way to robustify the attitude measurement \mathbf{y}_λ , the angular accelerations are compensated for by using the angular rate and linear velocity estimates as shown in (30), allowing for valid MPS measurements in the presence of centripetal accelerations, that occur even in trimming conditions such as helicoidal trajectories.

The theoretical stability and performance properties of the attitude and position filters derived in Section II cannot be directly inferred for the overall navigation system due to the filter coupling and to the use of pendular measurements in the attitude aiding observation. This limitation is a consequence of the adopted attitude aiding sensors, and stability and performance can be guaranteed in other experimental setups, e.g., by using non-pendular, vision-based attitude aiding sensors and by decoupling the attitude and position filters using external attitude reference units. For the proposed navigation system implementation, extensive Monte Carlo simulations showed that the architecture is stable in practice. The results of a set of Monte Carlo simulations used to validate the proposed navigation system is presented in Appendix B.

C. Multirate Filtering

In general, the GPS output rate is slower than the sampling rate of the inertial sensors. In this case, the position feedback gains are obtained by considering the multirate position filter as a periodic estimator, and adopting the optimality results for periodic systems derived in [43], which are briefly described in the ensuing for the position filter for the sake of clarity. Let the GPS and inertial sensors' sampling periods be denoted by T_{GPS} and T_{INS} , respectively, and define the ratio $n_T = T_{\text{GPS}}/T_{\text{INS}}$, $n_T \in \mathbb{N}$. The design system (6) is periodic with period n_T and is written in the compact form

$$\mathbf{x}_{k+1} = \mathbf{F}\mathbf{x}_k + \mathbf{G}\mathbf{w}_k, \quad \mathbf{y}_k = \mathbf{H}_k\mathbf{x}_k + \mathbf{v}_k \quad (34)$$

where $\mathbf{x}_k = [\mathbf{x}'_{\lambda k} \quad \mathbf{x}'_{b k}]'$, $\mathbf{w}_k = [\mathbf{w}'_{\omega k} \quad \mathbf{w}'_{b k}]'$, $\mathbf{y}_k = \mathbf{y}_{x k}$, $\mathbf{v}_k = \mathbf{v}_{\lambda k}$

$$\mathbf{F} = \begin{bmatrix} \mathbf{I} & -T\mathbf{I} \\ \mathbf{0} & \mathbf{I} \end{bmatrix}, \quad \mathbf{G} = \begin{bmatrix} -T\mathbf{I} & \mathbf{0} \\ \mathbf{0} & \mathbf{I} \end{bmatrix}$$

and the observation matrix of the system is given by

$$\mathbf{H}_k = \begin{cases} [\mathbf{I} & \mathbf{0}], & \text{if } \frac{k}{n_T} \in \mathbb{N}_0 \\ [\mathbf{0} & \mathbf{0}], & \text{otherwise.} \end{cases} \quad (35)$$

The system (34) can be associated with an augmented time-invariant system that models the dynamics of the state at time $k = in_T$, $i \in \mathbb{N}_0$, described by

$$\underline{\mathbf{x}}_{k+1} = \underline{\mathbf{F}}\underline{\mathbf{x}}_k + \underline{\mathbf{G}}\underline{\mathbf{w}}_k, \quad \underline{\mathbf{y}}_k = \underline{\mathbf{H}}\underline{\mathbf{x}}_k + \underline{\mathbf{D}}\underline{\mathbf{w}}_k + \underline{\mathbf{v}}_k \quad (36)$$

where the underlines denote the elements of the augmented state model, $\underline{\mathbf{x}}_k = \mathbf{x}_{kn_T}$, $\underline{\mathbf{x}}_k \in \mathbb{R}^6$

$$\begin{aligned} \underline{\mathbf{w}}_k &= [\mathbf{w}'_{kn_T} \quad \mathbf{w}'_{kn_T+1} \quad \cdots \quad \mathbf{w}'_{(k+1)n_T-1}]', \quad \underline{\mathbf{w}}_k \in \mathbb{R}^{6n_T} \\ \underline{\mathbf{v}}_k &= [\mathbf{v}'_{kn_T} \quad \mathbf{v}'_{kn_T+1} \quad \cdots \quad \mathbf{v}'_{(k+1)n_T-1}]', \quad \underline{\mathbf{v}}_k \in \mathbb{R}^{3n_T} \\ \underline{\mathbf{y}}_k &= [\mathbf{y}'_{kn_T} \quad \mathbf{y}'_{kn_T+1} \quad \cdots \quad \mathbf{y}'_{(k+1)n_T-1}]', \quad \underline{\mathbf{y}}_k \in \mathbb{R}^{3n_T} \end{aligned}$$

are the augmented noise and measurement vectors, respectively, and

$$\begin{aligned} \underline{\mathbf{F}} &= \mathbf{F}^{n_T}, \quad \underline{\mathbf{F}} \in \mathbb{M}(6, 6) \\ \underline{\mathbf{G}} &= [\mathbf{F}^{n_T-1}\mathbf{G} \quad \mathbf{F}^{n_T-2}\mathbf{G} \quad \cdots \quad \mathbf{G}], \quad \underline{\mathbf{G}} \in \mathbb{M}(6, 6n_T) \\ \underline{\mathbf{H}} &= [\mathbf{H}'_0 \quad \mathbf{F}'\mathbf{H}'_1 \quad \cdots \quad \mathbf{F}^{n_T-1}'\mathbf{H}'_{n_T-1}]', \quad \underline{\mathbf{H}} \in \mathbb{M}(3n_T, 6) \\ \underline{\mathbf{D}} &= \begin{bmatrix} \mathbf{0} & \mathbf{0} & \cdots & \cdots & \mathbf{0} \\ \mathbf{H}_1\mathbf{G} & \mathbf{0} & & & \vdots \\ \mathbf{H}_2\mathbf{F}\mathbf{G} & \mathbf{H}_2\mathbf{G} & \mathbf{0} & & \vdots \\ \vdots & & \ddots & \ddots & \vdots \\ \mathbf{H}_{n_T-1}\mathbf{F}^{n_T-1}\mathbf{G} & \cdots & \cdots & \mathbf{H}_{n_T-1}\mathbf{G} & \mathbf{0} \end{bmatrix} \\ \underline{\mathbf{D}} &\in \mathbb{M}(3n_T, 6n_T) \end{aligned}$$

which defines a time-invariant system, with correlated measurement and the state noises [43]. The optimal feedback gain for the time-invariant system (36) is given by

$$\mathbf{K} = [\underline{\mathbf{F}}\mathbf{P}\underline{\mathbf{H}}' + \underline{\mathbf{G}}\underline{\mathbf{\Xi}}\underline{\mathbf{D}}'] [\underline{\Theta} + \underline{\mathbf{D}}\underline{\mathbf{\Xi}}\underline{\mathbf{D}}' + \underline{\mathbf{H}}\mathbf{P}\underline{\mathbf{H}}']^{-1} \quad (37)$$

where $\mathbf{K} \in M(6, 3n_T)$, $\underline{\Xi} = E(\mathbf{w}_k \mathbf{w}_k')$, $\underline{\Theta} = E(\mathbf{v}_k \mathbf{v}_k')$, and $\underline{\mathbf{P}}$ is the steady-state optimal estimation error covariance matrix, given by the solution of the Riccati equation

$$\underline{\mathbf{P}} = \underline{\mathbf{F}}_* \underline{\mathbf{P}} \underline{\mathbf{F}}_*' + \underline{\mathbf{G}}_* \underline{\mathbf{G}}_*' - \underline{\mathbf{F}}_* \underline{\mathbf{P}} \underline{\mathbf{H}}' \underline{\mathbf{S}}^{-1} \underline{\mathbf{H}} \underline{\mathbf{P}} \underline{\mathbf{F}}_*'$$

where $\underline{\mathbf{S}} = \underline{\Theta} + \underline{\mathbf{D}} \underline{\Xi} \underline{\mathbf{D}}' + \underline{\mathbf{H}} \underline{\mathbf{P}} \underline{\mathbf{H}}'$, $\underline{\mathbf{G}}_* \underline{\mathbf{G}}_*' = \underline{\mathbf{G}} \underline{\Xi} \underline{\mathbf{G}}' - \underline{\mathbf{G}} \underline{\Xi} \underline{\mathbf{D}}' [\underline{\Theta} + \underline{\mathbf{D}} \underline{\Xi} \underline{\mathbf{D}}']^{-1} \underline{\mathbf{D}} \underline{\Xi} \underline{\mathbf{G}}'$ and $\underline{\mathbf{F}}_* = \underline{\mathbf{F}} - \underline{\mathbf{G}} \underline{\Xi} \underline{\mathbf{D}}' [\underline{\Theta} + \underline{\mathbf{D}} \underline{\Xi} \underline{\mathbf{D}}']^{-1} \underline{\mathbf{H}}$. Considering the partition of the feedback gain (37) given by $\underline{\mathbf{K}} = [K_0 \ K_1 \ \dots \ K_{n_T-1}]$, $\mathbf{K}_i \in M(6, 3)$, $i \in \mathbb{N}_0$, for the system (34)–(35), it can be easily shown that $\underline{\mathbf{D}} = \mathbf{0}$, $K_i = \mathbf{0}$, $i \neq 0$, and hence that the feedback gain $K_p = [K'_{1p} \ K'_{2p}]'$ is simply given by selecting the gain sub-matrix K_0 and propagating back to the time instant of the GPS measurement, i.e., $K_p = \mathbf{F}^{1-n_T} K_0$.

For further details on the synthesis of optimal estimators for discrete-time linear periodic systems, the reader is referred to [43] and references therein. A multirate filter channel to channel frequency analysis methodology can be found in [26].

IV. EXPERIMENTAL RESULTS

The proposed navigation system is validated in this section using a low-power hardware architecture enclosing low-cost sensors and mounted on-board the DELFIMx catamaran. The properties of the complementary filters in the frequency domain are discussed and the resulting performance of the filters is analyzed. The attitude and position estimation results using the experimental data collected in the catamaran sea tests are presented, and the usual cases of GPS signal outage and of initial calibration error of the rate gyro bias are addressed.

A. Ocean Craft and Sensor Characteristics

The DELFIMx craft, depicted in Fig. 1, is a small Catamaran 4.5 m long and 2.45 m wide, with a mass of 300 Kg. Propulsion is ensured by two propellers driven by electrical motors, and the maximum rated speed of the vehicle with respect to the water is 6 knots. For integrated guidance and control, a path-following control strategy was adopted due to its enhanced performance, which translates into smoother convergence to the path and less demand on the control effort [2]. The vehicle has a wing shaped, central structure that is lowered during operations at sea. At the bottom of this structure, a low drag body is installed that can carry acoustic transducers. For bathymetric operations and sea floor characterization, the wing is equipped with a mechanically scanned pencil beam sonar and a sidescan sonar.

The DELFIMx hardware architecture developed by the ISR-IST is a self-contained system mounted on three cases which can be fit into and removed from the autonomous surface craft (ASC). The most sensitive parts are vibration isolated from the hull using a soft suspension mechanism, which acts as a low pass mechanical filter that provides further attenuation of the ASC vibration on the electronics. The hardware architecture is built around the low-cost low-power floating point Digital Signal Processor (DSP) TI TMS320C33, displayed in Fig. 6, which is connected to the data acquisition hardware through a dual port RAM expansion board developed by IST-ISR. Special

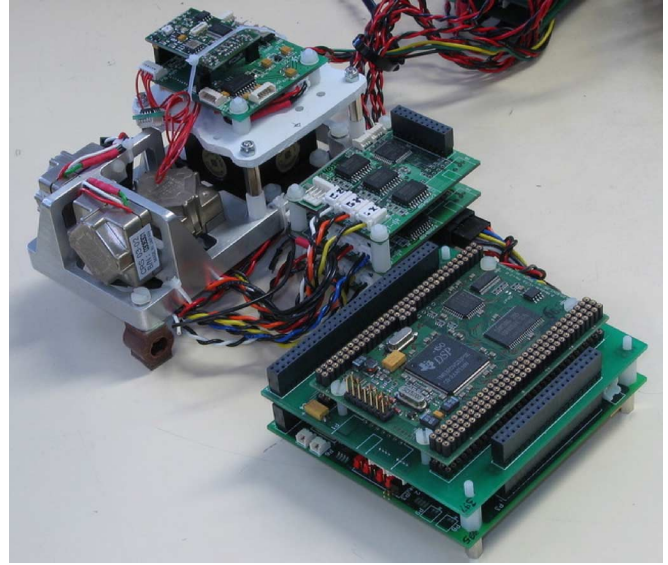


Fig. 6. Hardware architecture.

care was taken during the electronics development in order to implement measures that improve the electromagnetic compatibility (EMC). The data acquisition distributed architecture was built around the controller area network (CAN) industrial real time network, for control and navigation purposes and on 100 MB/s Ethernet for payload data interface. A series of very low-power boards designed at ISR using the Phillips XAS3 16 bit microcontroller, and the ATMEL AT90CAN128 8-bit AVR Flash microcontroller with extended CAN capabilities are used to interface all sensors and exchange data through the CAN Bus. In this architecture the TMS320C33 schedules all Guidance, Control, and Navigation tasks to meet their deadlines. Finally, a PC104 board connected to the CAN Bus and to Ethernet runs the mission control system and implements a blackbox where relevant data generated by the ASC are properly saved in a solid state disk for post-mission analysis.

The IMU on-board the DELFIMx craft is a strap-down system comprising a triaxial XBOW CXL02LF3 accelerometer and three single axes Silicon Sensing CRS03 rate gyros mounted along three orthogonal axes. These sensors are attached orthogonally to a custom made stand that is presented in the left side of Fig. 6 with the sensors assembled. The inertial sensors are sampled at 56 Hz using six Texas ADS1210 directly connected to a microcontroller board. The ADS1210 is a high precision, wide dynamic range, delta-sigma analog-to-digital converter with 24-bit resolution operating from a single +5 V supply. The differential inputs are ideal for direct connection to transducers guaranteeing 20 bits of effective resolution which is a suitable accuracy for the set of inertial sensors used in the present application.

The hardware architecture is also equipped with a Honeywell HMR3300 magnetometer, interfaced by a serial port connection with a sampling rate of 8 Hz. Due to the distinct sampling rates of the magnetometer and inertial sensors, a multirate formulation similar to that described in Section III-C is adopted for the yaw estimation. The GPS receiver installed on board the DELFIMx is a Thales Navigation DG14 receiver

TABLE I
 COMPLEMENTARY FILTER PARAMETERS

	State Weights	Observation Weight	Filter Gain
Attitude Filter	$\Xi_\omega = 3\mathbf{I}$ $\Xi_b = 10^{-10}\mathbf{I}$	$\Theta_\lambda = 0.8 \times 10^{-2}\mathbf{I}$	$K_{1\lambda} = 2.97 \times 10^{-1}\mathbf{I}$ $K_{2\lambda} = 9.41 \times 10^{-5}\mathbf{I}$
Position Filter	$\Xi_p = 5 \times 10^{-2}\mathbf{I}$ $\Xi_a = 10\mathbf{I}$	$\Theta_p = \mathbf{I}$	$K_{1p} = 0.59\mathbf{I}$ $K_{2p} = 0.14\mathbf{I}$

which presents an accuracy of 3.0 m Circular Error Probable (CEP) in autonomous mode and 0.40 m in differential mode. In the present work, the GPS works in autonomous mode and the measurements are provided at a 4 Hz sampling rate.

B. Filter Parameter Design

The attitude and position filters derived in Section II are designed to produce a closed-loop frequency response which blends the complementary frequency contents of the inertial and the aiding sensor measurements. In this frequency domain framework, the state and measurement weight matrices are used as tuning parameters and the filter gains are identified with the steady-state Kalman filter gains. The adopted weights and corresponding gains are detailed in Table I.

The complementary frequency response of the closed-loop filters is depicted in Fig. 7 and was obtained by considering $\mathbf{Q}(\bar{\lambda}) = \mathbf{Q}(0)$ and $\bar{\mathcal{R}}_k = \mathbf{I}$, i.e., the frequency response of the time invariant systems (6) and (19) used in the filter design. As shown in Fig. 7, the low-frequency region of the MPS and GPS are blended with the high-frequency contents of the open-loop integration of the inertial measurements, which is given by

$$\begin{aligned} \lambda_{\omega k+1} &= \lambda_{\omega k} + T\mathbf{Q}(0)\boldsymbol{\omega}_{r k}, \\ \mathbf{p}_{a k+1} &= \mathbf{p}_{a k} + T\mathbf{v}_{a k} + \frac{T^2}{2}\mathbf{a}_{r k}, \quad \mathbf{v}_{a k+1} = \mathbf{v}_{a k} + T\mathbf{a}_{r k}. \end{aligned}$$

The sum of the transfer functions of the filters, depicted in Fig. 7, is unitary, which shows that the adopted steady-state Kalman gains bear complementary filters, as expected. The obtained complementary transfer functions are validated in practice with the experimental data obtained on-board the DELFIMx catamaran.

As discussed in Section II-A, the proposed attitude filter is identified with the steady-state Kalman filter for constant pitch and roll angles and, in case of time-varying pitch and roll angles, the performance degradation can be analyzed using the covariance propagation equations detailed in Appendix A. A numerical comparison of the Kalman and the obtained estimation error covariances is shown in Fig. 8, considering the design weights presented in Table I. As shown in Fig. 8(b), the estimation error covariance of the proposed attitude complementary filter is less than 1% above the optimal estimation error covariance for the aggressive pitch and roll trajectory depicted in Fig. 8(a).

C. Experimental Results Analysis

This section presents the navigation system estimation results obtained with the experimental data collected on-board the DELFIMx catamaran during tests at sea using the hardware architecture detailed previously. The trajectory of the vehicle is presented in Fig. 9, where a green line is used to depict the

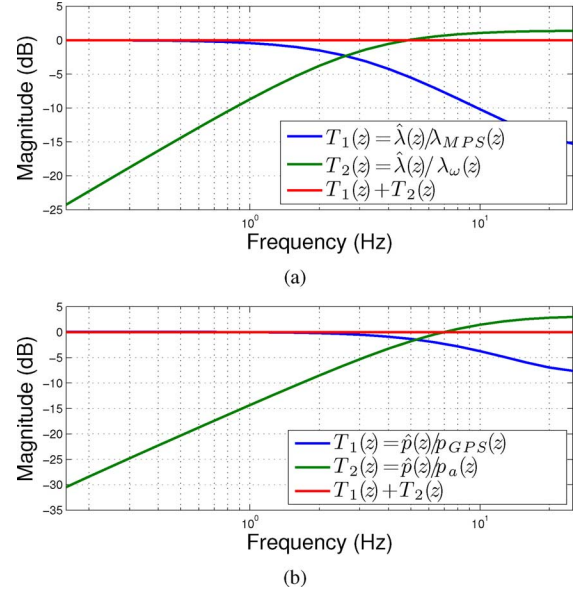
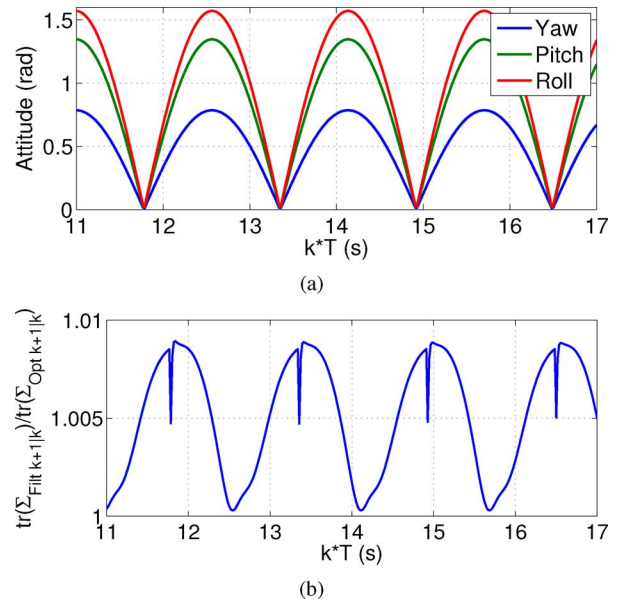


Fig. 7. Complementary filter transfer functions. (a) Attitude filter. (b) Position filter.


 Fig. 8. Attitude filter performance ($T = 1/5$ s). (a) Attitude. (b) Error covariance ratio $\text{tr}(\Sigma_{\text{Filter}})/\text{tr}(\Sigma_{\text{Optimal}})$.

filter estimates and a wide blue line represents the GPS measurements. As depicted in Fig. 9(a), the trajectory described by the DELFIMx vehicle is mainly characterized by straight line and circular paths, to assess the performance of the navigation system in realistic operational scenarios.

The attitude estimation results, presented in Fig. 10, are according to the maneuvers described by the robotic platform, whose forward velocity is mainly along the body frame x -axis, and hence describes mostly yaw turns. The yaw estimate depicted in Fig. 10(a) is consistent with the turning maneuvers and the heading directions of the straight paths performed by the platform, illustrated in Fig. 9(a), and with the yaw measurement given by the GPS unit. Clearly, the filter estimate is more

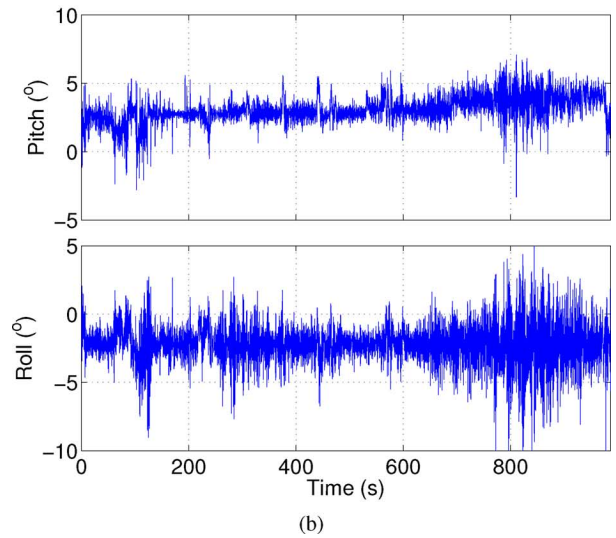
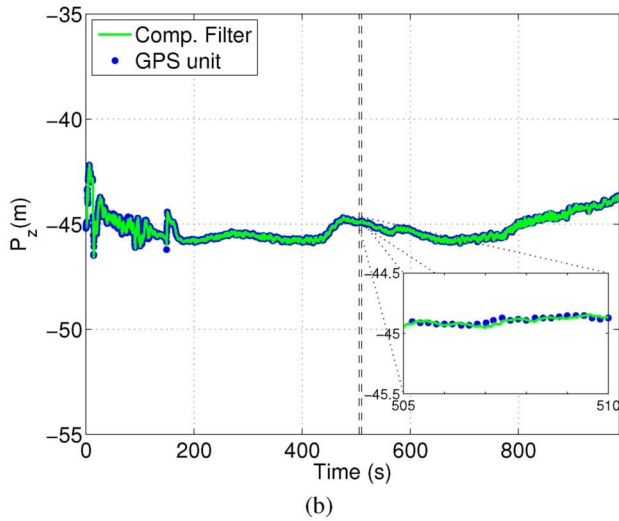
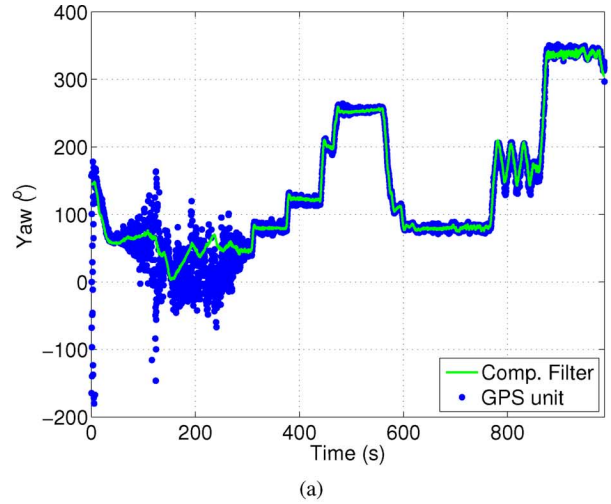
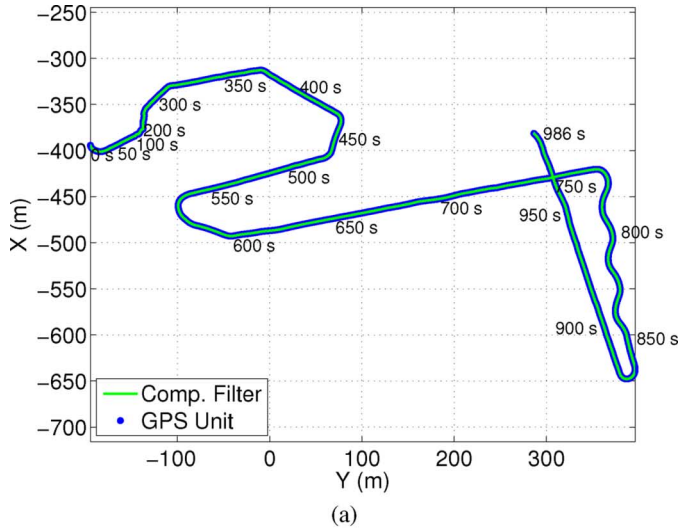


Fig. 9. DELFIMx trajectory estimation results. (a) xy -plane projection. (b) z -axis estimate, with a subplot box showing the estimation results for $t \in [505 \ 510]$ s.

Fig. 10. Attitude estimation results. The GPS yaw measurements are external to the filtering algorithm, and depicted solely for the sake of comparison. (a) Yaw. (b) Pitch and roll.

accurate than the GPS yaw measurement, that is used only for the sake of validation of the estimation results and is not fed to the filter. The yaw measurement of the GPS unit is degraded for small velocities, as shown in Fig. 10(a) for the time interval $t \in [50 \ 300]$ s where the platform maneuver is characterized by small forward velocity, as presented in Fig. 11(b).

The pitch and roll angles, presented in Fig. 10(b), oscillate around the mean values of 3.08° and -2.20° , respectively, that correspond approximately to the installation angles of the hardware architecture. Pitch and roll fluctuations occur due to platform turning, interference of waves, and vibration of the hull due to the propellers. Larger oscillations are verified when the vehicle turns, for example the slalom trajectory at $[760 \ 880]$ s bears larger peak to peak values of the pitch and roll angles, due to the oscillation of the catamaran while performing the maneuver, and to the vibration induced by the propellers. The pitch and roll values satisfy the conditions under which the stability propositions derived in Sections II hold. Interestingly enough, the standard deviations of the pitch and roll estimates are 0.95° and 1.42° , respectively, which suggests that the performance

degradation of the attitude filter due to time-varying pitch and roll is small for the present application.

The velocity estimation results are shown in Fig. 11. The proposed filter is based on the attitude kinematics and hence does not estimate explicitly the angular velocity, in spite of compensating for the rate gyro noise and bias to estimate attitude. The angular velocity estimate, presented in Fig. 11(a), is given by the rate gyro measurements, compensated with the bias estimate, and is presented to verify the consistency of the attitude estimates. The z -axis angular velocity is synchronous with the yaw changes in Fig. 10(a), namely in the initial turn, and in turning maneuvers at the time intervals where variations in the angular velocity are verified, such as $[305 \ 315]$ s, $[370 \ 380]$ s, $[435 \ 450]$ s, $[465 \ 470]$ s, $[560 \ 600]$ s, and $[760 \ 880]$ s. These turning maneuvers can be identified in Fig. 9(a) by analyzing the time tags. The x - and y -axes angular velocities are consistent with the pitch and roll estimates, i.e., are approximately zero mean and the most noticeable fluctuation occurs at the slalom maneuver at $[760 \ 880]$ s.

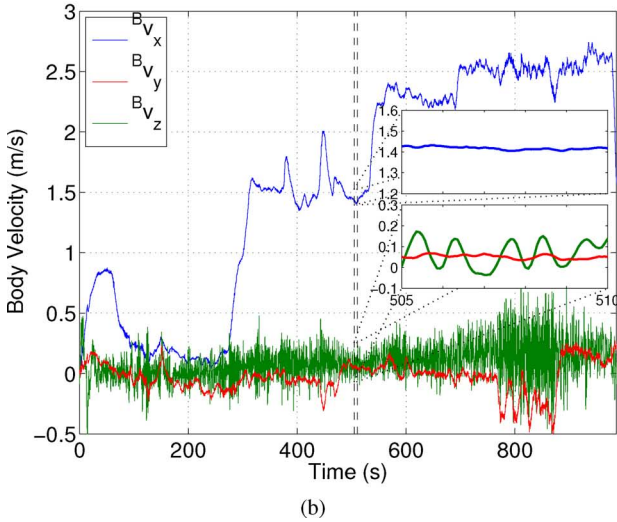
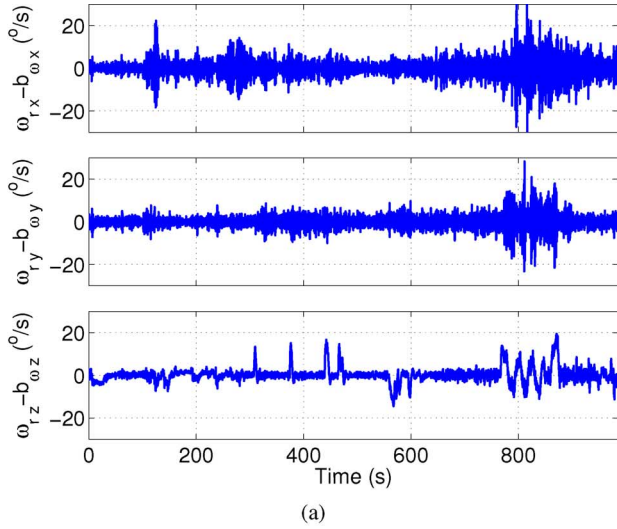


Fig. 11. Linear and angular velocity estimation results. (a) Angular velocity. (b) Linear velocity, with subplot boxes showing the estimation results for $t \in [505\ 510]$ s.

The estimate of the linear velocity, expressed in body coordinates, is shown in Fig. 11(b). The x -axis body velocity is positive and approximately stepwise constant at the straight paths trajectories at the time intervals $[320\ 365]$ s, $[385\ 430]$ s, $[480\ 550]$ s, $[615\ 750]$ s and $[880\ 980]$ s. The y -axis body velocity is approximately zero-mean during straight path trajectories, and centrifugal during turning maneuvers due to sideslip of the catamaran, as evidenced for the slalom maneuver results, see Fig. 11(b) and detail in Fig. 12. Also, the mean of the y -axis body velocity is nonzero when the vehicle is subject to external, Earth fixed forces such as waves induced by nearby vessels and oceanic currents, such as in the time interval $[760\ 980]$ s. The z -axis body velocity is approximately zero-mean, as expected for an oceanic platform.

The duration of the mission is large with respect to the oceanic disturbances acting on the catamaran's hull, such as waves, that produce short term oscillating motion, hardly distinguishable from sensor noise when the interval $t \in [0\ 980]$ s is considered. To analyze the filter estimates more closely, estimation results for the time interval $t \in [505\ 510]$ s, where

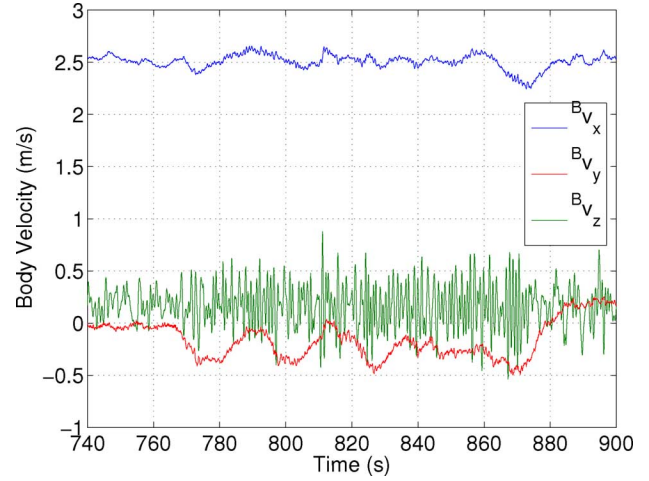


Fig. 12. Linear velocity during the slalom maneuver at $[760\ 880]$ s.

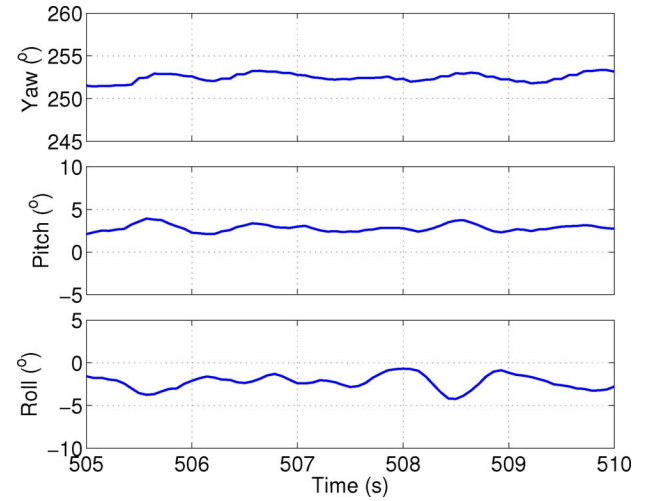


Fig. 13. Attitude estimation results for $t \in [505\ 510]$ s.

the vehicle describes a straight line trajectory, are depicted in Fig. 13 and in the subplot boxes presented in Figs. 9(b) and 11(b). The mean values of the yaw, pitch, and roll angles shown in Fig. 13 are coherent with the vehicle's heading and the hardware installation angles, and the angular fluctuations are naturally induced by the swaying of the vehicle. The vehicle estimation results presented in the subplots of Fig. 11(b) show that the x - and y -components of the velocity estimates are smooth and approximately constant, and that the z -axis velocity oscillates mostly due the impact of short period ocean waves on the vehicle's hull. The subplot presented in Fig. 9(b) shows that the position estimates is a blend of the inertial and the GPS unit readings, since it is smooth and diverse from the GPS measurements.

The rate gyro bias estimation results are presented in Fig. 14(a). The results show that the attitude complementary filter compensates for slowly time-varying bias, by means of the small design weight Ξ_b in the computation of the feedback gain, see Table I for details. However, the Kalman gains are stationary and the initial bias uncertainty should be close to the steady-state bias covariance, i.e., the bias calibration error should be small. As shown in Fig. 14(b), using a larger

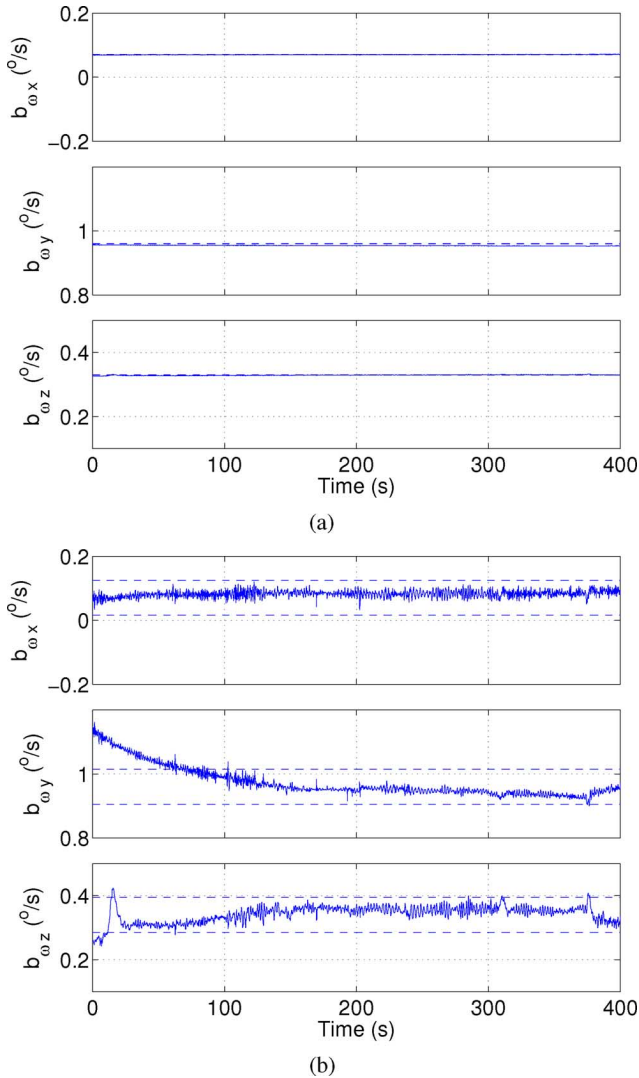


Fig. 14. Rate gyro bias estimation. The dashed lines show the $\pm 3\sqrt{\Xi_b}$ bounds around the true bias. (a) Compensation of slowly time-varying bias, $\Xi_b = 10^{-10}$. (b) Calibration error compensation, $\Xi_b = 10^{-7}$.

design weight Ξ_b enables the filter to compensate for the bias calibration error at the cost of larger steady state covariance. Consequently, the tradeoff between the accuracy of the bias estimate and the compensation of large bias estimation errors should be considered in the design process. Usual mission requirements include bias calibration during system warm-up, where bias fluctuations are large, and compensation of long term, slowly time-varying bias changes during the course of the mission. A simple gain switching technique can be adopted, using a large design weight Ξ_b during the initialization of the system, and a smaller Ξ_b in the long term.

The position estimation results are coherent with the GPS measurements, as evidenced in Fig. 9. To analyze the weight of GPS aiding in the filter estimation results, the case of GPS outage is considered by canceling the GPS measurement feedback at selected time intervals when the vehicle turns or enters long straight paths. The GPS outage time instants are detailed in Table II, and the corresponding trajectories are illustrated in Fig. 15(a). The navigation system results presented in Table II

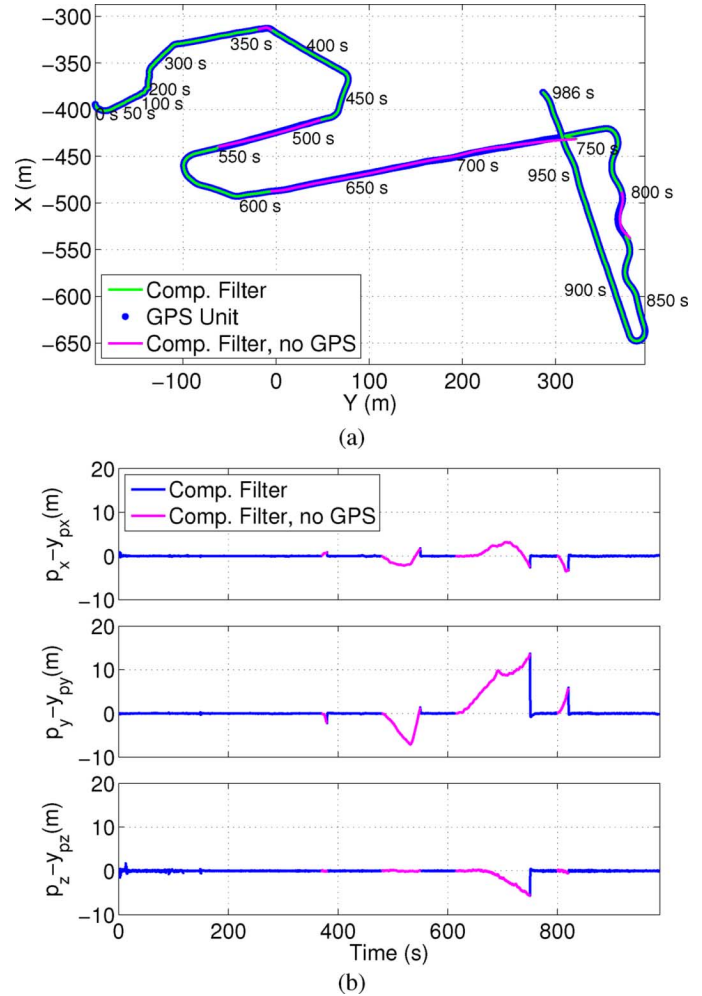


Fig. 15. DELFIMx trajectory estimation results (GPS signal jamming). (a) xy -plane projection. (b) Difference between the estimated and the GPS measured positions.

TABLE II
GPS OUTAGE RESULTS

Time Interval	Final Position Drift (m)	Average Position Drift (m/s)
[370 380] s	2.38	0.238
[480 550] s	1.91	0.027
[615 750] s	15.37	0.114
[800 820] s	7.14	0.357

show that the position drift rate is small during GPS signal outage. Consequently, the position filter operates without relying too much on the GPS position observations, by exploiting the inertial measurements information. The navigation system follows closely the straight path trajectories, and successfully exploits the angular information during the turning maneuvers. The position estimates are bounded for the GPS outage time intervals, as shown in Fig. 15(b), however position error buildup occurs due to the open-loop integration of the accelerometers, combined with pitch and roll estimation errors that induce position estimate drift, as expected.

The frequency domain validation of the complementary transfer functions is performed using the MATLAB spectrogram function to compute the short-time Fourier transform of the position and attitude estimates, aiding sensor measurements,

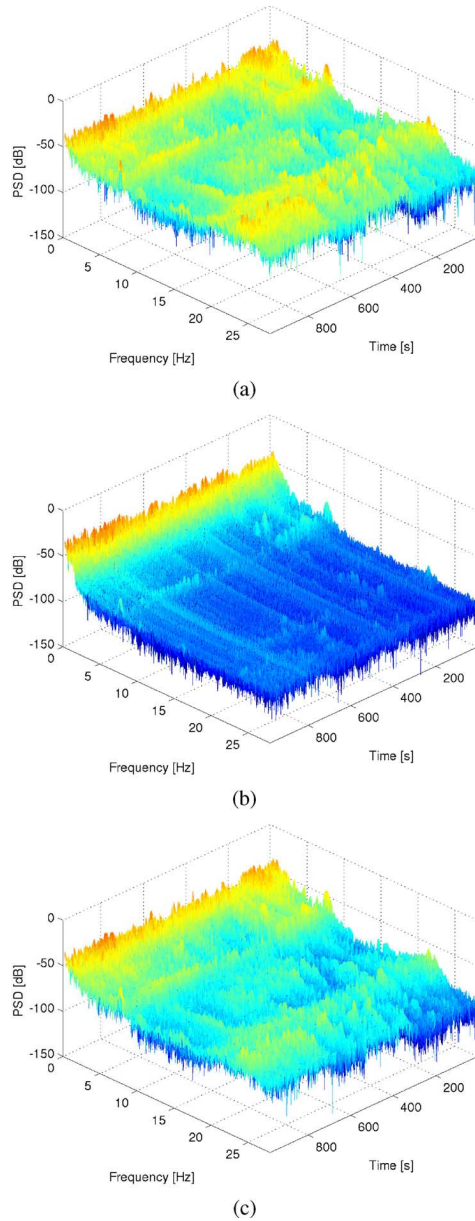


Fig. 16. Spectrograms of the pitch measurements and filter estimate. (a) Aiding measurement (MPS). (b) Rate gyro integration. (c) Filter estimate.

and inertial sensor measurements integration. The short-time Fourier transform computes a time-dependent Fourier transform of the signal multiplied by a sliding window function, and allows for a characterization of the time-varying frequency contents of a signal at each time instant [44]. The choice of the window function size is a trade-off between good resolution in the time domain (short window), and good resolution in the frequency domain (large window).

Using a Hamming window of length 512 and 500 overlapping segments, the frequency contents of the attitude and position signals can be analyzed, and the blending of the low frequency contents of the aiding sensors with the high frequency contents of the inertial sensor integration can be studied. Namely, Fig. 16 illustrates the fusion in the frequency domain of the pendular measurements with the inertial readings. Although a rigorous

analysis in the frequency domain using the spectrogram is precluded by the multirate formulation of the navigation system, it is possible to verify qualitatively that the sensor measurements are blended using complementary transfer functions. The low-frequency contents of the pitch observations presented in Fig. 16(a) are blended with the high-frequency contents of the open-loop integration of the inertial measurements, shown in Fig. 16(b), producing the attitude estimate with the frequency contents depicted in Fig. 16(c). Qualitatively, it is verified that the filter estimates are similar to the aiding sensor measurements, smoothed by the inertial measurement integration. This blending in the frequency domain of the aiding and inertial sensors data is according to the complementary transfer functions depicted in Fig. 7 and derived in Section IV-B.

The experimental results obtained on-board the DELFIMx catamaran validate the proposed navigation system architecture. The adopted design parameters yield the desired sensor fusion in the frequency domain, and produce good attitude and position estimation and rate gyro bias compensation results in the time domain. The attitude and position estimates were consistent with the trajectory profile, and the navigation system endured GPS outage, which shows that the proposed complementary filter based architecture is suitable for the oceanic application under study.

V. CONCLUSION

Complementary filters for attitude and position estimation were proposed, and their stability and performance properties were derived theoretically. Using the Euler angles parametrization, the attitude filter compensates for rate gyro bias and is stable for trajectories described by nonsingular configurations. The position filter estimates velocity in body coordinates and position in Earth frame, and is asymptotically stable. The attitude and position complementary filters were integrated to produce a complete navigation system, whose structure can be represented in a simple block diagram and can be easily implemented on a low-cost, low-power consumption hardware. The filter gains are computed using frequency domain design to shape a frequency response that exploits the low-frequency contents of the aiding sensors and the high-frequency contents of the inertial sensors. Implementation aspects were detailed, namely an attitude aiding observation based on magnetic and pendular measurements was derived, and the problem of multiple sampling rates was tackled using optimal results for periodic systems. The navigation system was validated using experimental data, in tests at sea with the DELFIMx catamaran. Rate gyro bias was compensated for, and good attitude and position estimates were obtained by exploiting the complementary frequency contents of the aiding and the inertial sensors. Also, the navigation system was shown to yield accurate results and small drift in the case of GPS outage.

Stability and performance properties were derived separately for the proposed attitude and position filters. Future work will address the generalization of these properties to the overall navigation system, and analyze the cross-correlations between the attitude and velocity estimates. Also, advanced compensation of sensor errors can be addressed to further enhance the estimation results. Namely, the position aiding computed by the GPS unit

was successfully integrated in the filter, however future work should address the dynamic compensation of GPS pseudorange measurement errors (tightly coupled configuration); and the off-line accelerometer bias calibration was found suitable for the duration of the ASC mission, nonetheless online accelerometer bias compensation is of interest for future applications.

APPENDIX A

PERFORMANCE OF THE ATTITUDE FILTER

The system (7) can be written in the compact form as

$$\begin{bmatrix} \tilde{\lambda}_{k+1} \\ \tilde{\mathbf{b}}_{k+1} \end{bmatrix} = (\mathbf{F}_k - \mathbf{K}_k \mathbf{H}_k) \begin{bmatrix} \tilde{\lambda}_k \\ \tilde{\mathbf{b}}_k \end{bmatrix} + \mathbf{G}_k \begin{bmatrix} \mathbf{w}_{\omega k} \\ \mathbf{w}_{b k} \end{bmatrix} - \mathbf{K}_k \mathbf{Q}(\tilde{\lambda}_{k-1}) \mathbf{v}_{\lambda k},$$

where

$$\begin{aligned} \mathbf{F}_k &= \begin{bmatrix} \mathbf{I} & -T\mathbf{Q}(\tilde{\lambda}_k) \\ \mathbf{0} & \mathbf{I} \end{bmatrix} \\ \mathbf{G}_k &= \begin{bmatrix} -T\mathbf{Q}(\tilde{\lambda}_k) & \mathbf{0} \\ \mathbf{0} & \mathbf{I} \end{bmatrix} \\ \mathbf{K}_k &= \begin{bmatrix} \mathbf{Q}(\tilde{\lambda}_k)(K_{1\lambda} - \mathbf{I})\mathbf{Q}^{-1}(\tilde{\lambda}_{k-1}) + \mathbf{I} \\ K_{2\lambda}\mathbf{Q}^{-1}(\tilde{\lambda}_{k-1}) \end{bmatrix} \\ \mathbf{H}_k &= [\mathbf{I} \quad \mathbf{0}]. \end{aligned}$$

The estimation error covariance, denoted by

$$\Sigma_{k+1|k} = E \left(\begin{bmatrix} \tilde{\lambda}_{k+1} \\ \tilde{\mathbf{b}}_{k+1} \end{bmatrix} \begin{bmatrix} \tilde{\lambda}'_{k+1} & \tilde{\mathbf{b}}'_{k+1} \end{bmatrix} \right)$$

satisfies the propagation equation [34]

$$\begin{aligned} \Sigma_{k+1|k} &= (\mathbf{F}_k - \mathbf{K}_k \mathbf{H}_k) \Sigma_{k|k-1} (\mathbf{F}_k - \mathbf{K}_k \mathbf{H}_k)' \\ &+ \mathbf{G}_k \Xi \mathbf{G}_k' + \mathbf{K}_k \mathbf{Q}(\tilde{\lambda}_{k-1}) \Theta \mathbf{Q}(\tilde{\lambda}_{k-1})' \mathbf{K}_k'. \end{aligned} \quad (38)$$

The estimation error covariance of the Kalman filter for the attitude kinematics (4), denoted by $\mathbf{P}_{k+1|k}$, satisfies

$$\begin{aligned} \mathbf{P}_{k+1|k} &= \mathbf{F}_k \mathbf{P}_{k|k-1} \mathbf{F}_k' + \mathbf{G}_k \Xi \mathbf{G}_k' \\ &- \mathbf{F}_k \mathbf{P}_{k|k-1} \mathbf{H}_k' \mathbf{S}_P^{-1} \mathbf{H}_k \mathbf{P}_{k|k-1} \mathbf{F}_k' \end{aligned} \quad (39)$$

where $\mathbf{S}_P k = \mathbf{H}_k \mathbf{P}_{k|k-1} \mathbf{H}_k' + \Theta$. The performance of the proposed attitude filter can be studied offline by comparing the estimation error covariance given by (38) with the optimal error covariance described by (39), as illustrated in the analysis presented in Section IV.

APPENDIX B

MONTE CARLO SIMULATION RESULTS

This section summarizes the Monte Carlo simulation results that validated the proposed navigation system, prior to the experimental tests presented in Section IV. The simulation parameters were defined according to characteristics of the hardware architecture described in Section IV-A. The Gaussian white-noise covariances of the measurements ω_r , \mathbf{a}_r , \mathbf{m}_r , and \mathbf{y}_p were, respectively, $0.18\mathbf{I}^\circ/\text{s}$, $2.6 \times 10^{-3}\mathbf{I}\text{m}/\text{s}^2$, $\mathbf{I}\text{mG}$, and $3\mathbf{I}\text{m}$, and $\mathbf{b}_\omega = 0.05 \begin{bmatrix} 1 & 1 & 1 \end{bmatrix}^\circ/\text{s}$. The complementary Kalman filters were executed at 56 Hz, the inertial sensors were sampled at

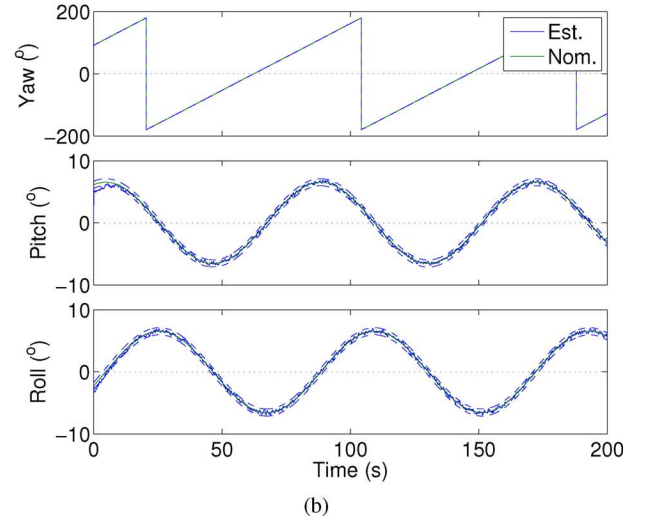
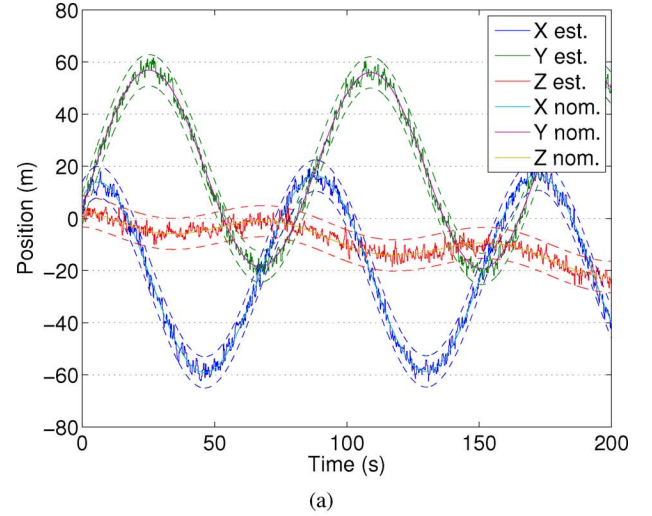


Fig. 17. Monte Carlo simulation results. (a) Nominal and estimated position (3- σ bounds are shown using dashed lines). (b) Nominal and estimated attitude (3- σ bounds are shown using dashed lines).

TABLE III
COMPLEMENTARY FILTER ESTIMATION RESULTS
(MONTE CARLO SIMULATIONS)

Estimation Error	Mean Standard Deviation
$\hat{\mathbf{p}} - \bar{\mathbf{p}}$	$\begin{bmatrix} 2.01 & 2.01 & 2.01 \end{bmatrix} \text{ m}$
$\hat{\lambda} - \bar{\lambda}$	$\begin{bmatrix} 0.03 & 0.19 & 0.19 \end{bmatrix} ^\circ$
$\hat{\mathbf{v}} - \bar{\mathbf{v}}$	$\begin{bmatrix} 0.46 & 0.46 & 0.46 \end{bmatrix} \text{ m/s}$
$\hat{\mathbf{b}}_\omega - \bar{\mathbf{b}}_\omega$	$\begin{bmatrix} 1.56 \times 10^{-3} & 1.69 \times 10^{-3} & 1.27 \times 10^{-3} \end{bmatrix} ^\circ/\text{s}$

the filter's rate, and the GPS position measurements were obtained at 4 Hz. The filter gains were designed using the synthesis weights adopted in the experimental tests, presented in Table I. The disturbances found in the experimental setup are usually non-Gaussian and correlated in time, which motivates the design of gains in the frequency domain, that yields the complementary filter transfer functions presented in Section IV-B.

The proposed navigation system was studied in simulation for an upwards trimming trajectory, subject to constant centripetal acceleration. A set of 500 Monte Carlo simulations was run, using a Gaussian distribution model for the initial conditions. The standard deviation matrices for the initial conditions

$\mathbf{p}(t_0)$, $\boldsymbol{\lambda}(t_0)$, $\mathbf{v}(t_0)$, and $\boldsymbol{\omega}(t_0)$ were $3\mathbf{I}$ m, $5\mathbf{I}^\circ$, $0.5\mathbf{I}$ m/s, and $0.285\mathbf{I}^\circ/\text{s}$, respectively.

The estimation results are presented in Table III and show that the attitude and position estimates are more accurate than those obtained by using solely the aiding sensors. Position and attitude estimation results for a single Monte Carlo, and the standard deviations of the Monte Carlo simulations set, are illustrated in Fig. 17(a) and (b), respectively, which show that the estimation errors remain bounded over time. The proposed navigation system was stable for all the Monte Carlo runs, as expected.

REFERENCES

- [1] C. Silvestre, P. Oliveira, A. Pascoal, L. G. Silva, J. A. Santos, and M. da G. Neves, "Inspection and diagnosis of the Sines West breakwater," presented at the 29th Int. Conf. Coastal Eng. (ICCE), Lisbon, Portugal, Sep. 2004.
- [2] P. Gomes, C. Silvestre, A. Pascoal, and R. Cunha, "A coastline following preview controller for the DELFIMx vehicle," presented at the 17th Int. Offshore Polar Eng. Conf. Exhibition, Lisbon, Portugal, 2007.
- [3] K. R. Britting, *Inertial Navigation Systems Analysis*. New York: Wiley, 1971.
- [4] J. L. Crassidis, F. L. Markley, and Y. Cheng, "Survey of nonlinear attitude estimation methods," *J. Guid., Control, Dyn.*, vol. 30, no. 1, pp. 12–28, Jan.-Feb. 2007.
- [5] J. C. Kinsey, R. M. Eustice, and L. L. Whitcomb, "A survey of underwater vehicle navigation: Recent advances and new challenges," presented at the 7th IFAC Conf. Manoeuvring Control Marine Craft (MCMC), Lisbon, Portugal, 2006.
- [6] F. L. Markley, "Attitude error representations for Kalman filtering," *J. Guid., Control, Dyn.*, vol. 26, no. 2, pp. 311–317, Mar.-Apr. 2003.
- [7] M. E. Pittelkau, "Rotation vector in attitude estimation," *J. Guid., Control, Dyn.*, vol. 26, no. 6, pp. 855–860, Nov.-Dec. 2003.
- [8] G. Dissanayake, S. Sukkarieh, E. Nebot, and H. Durrant-Whyte, "The aiding of a low-cost strapdown inertial measurement unit using vehicle model constraints for land vehicle applications," *IEEE Trans. Robot. Autom.*, vol. 17, no. 4, pp. 731–747, Oct. 2001.
- [9] S. J. Julier and J. K. Uhlmann, "Unscented filtering and nonlinear estimation," *Proc. IEEE*, vol. 92, no. 3, pp. 401–422, Mar. 2004.
- [10] J. L. Crassidis, "Sigma-point Kalman filtering for integrated GPS and inertial navigation," *IEEE Trans. Aerosp. Electron. Syst.*, vol. 42, no. 2, pp. 750–756, Apr. 2006.
- [11] A. K. Sanyal, T. Lee, M. Leok, and N. H. McClamroch, "Global optimal attitude estimation using uncertainty ellipsoids," *Syst. Control Lett.*, vol. 57, no. 3, pp. 236–245, 2008.
- [12] R. Mahony, T. Hamel, and J.-M. Pflimlin, "Nonlinear complementary filters on the special orthogonal group," *IEEE Trans. Autom. Control*, vol. 53, no. 6, pp. 1203–1218, Jun. 2008.
- [13] N. Metni, J.-M. Pflimlin, T. Hamel, and P. Souères, "Attitude and gyro bias estimation for a VTOL UAV," *Control Eng. Practice*, vol. 14, no. 12, pp. 1511–1520, 2006.
- [14] H. Rehbinder and B. K. Ghosh, "Pose estimation using line-based dynamic vision and inertial sensors," *IEEE Trans. Autom. Control*, vol. 48, no. 2, pp. 186–199, Feb. 2003.
- [15] H. Rehbinder and X. Hu, "Nonlinear state estimation for rigid body motion with low-pass sensors," *Syst. Control Lett.*, vol. 4, no. 3, pp. 183–190, Jul. 2000.
- [16] J. F. Vasconcelos, C. Silvestre, and P. Oliveira, "A landmark based nonlinear observer for attitude and position estimation with bias compensation," presented at the 17th IFAC World Congr., Seoul, Korea, Jul. 2008.
- [17] N. Wiener, *Extrapolation, Interpolation and Smoothing of Stationary Time Series*. New York: Wiley, 1949.
- [18] R. G. Brown, "Integrated navigation systems and Kalman filtering: A perspective," *J. Inst. Navigation*, vol. 19, no. 4, pp. 355–362, 1972.
- [19] R. G. Brown and P. Y. C. Hwang, *Introduction to Random Signals and Applied Kalman Filtering*, 3rd ed. New York: Wiley, 1997.
- [20] W. T. Higgins, "A comparison of complementary and Kalman filtering," *IEEE Trans. Aerosp. Electron. Syst.*, vol. AES-11, no. 3, pp. 321–325, May 1975.
- [21] Y. Bar-Shalom, X. R. Li, and T. Kirubarajan, *Estimation with Applications to Tracking and Navigation*. New York: Wiley-Interscience, 2001.

- [22] S. Merhav, *Aerospace Sensor Systems and Applications*. New York: Springer-Verlag, 1998.
- [23] M. Kayton and W. R. Fried, *Avionics Navigation Systems*, 2nd ed. New York: Wiley-Interscience, 1997.
- [24] X. Yun, E. R. Bachmann, R. McGhee, R. H. Whalen, R. L. Roberts, R. G. Knapp, A. J. Healey, and M. J. Zyda, "Testing and evaluation of an integrated GPS/INS system for small AUV navigation," *J. Ocean. Eng.*, vol. 24, no. 3, pp. 396–404, Jul. 1999.
- [25] L. L. Whitcomb, D. R. Yoerger, and H. Singh, "Combined Doppler/LBL based navigation of underwater vehicles," presented at the 11th Int. Symp. Unmanned Untethered Submersible Technol., Durham, NH, Aug. 1999.
- [26] A. Pascoal, I. Kaminer, and P. Oliveira, "Navigation system design using time varying complementary filters," *IEEE Aerosp. Electron. Syst.*, vol. 36, no. 4, pp. 1099–1114, Oct. 2000.
- [27] J. Roberts, P. Corke, and G. Buskey, "Low-cost flight control system for a small autonomous helicopter," in *Proc. IEEE Int. Conf. Robot. Autom.*, Taipei, Taiwan, Sep. 2003, pp. 546–551.
- [28] S. Park, "Avionics and control system development for mid-air rendezvous of two unmanned aerial vehicles," Ph.D. dissertation, Dept. Aeronautics Astronautics, Massachusetts Inst. Technol., Boston, 2004.
- [29] D. Jung and P. Tsiotras, in *AIAA Infotech Aerosp.*, Rohnert Park, CA, May 2007.
- [30] J. J. Craig, *Introduction to Robotics: Mechanics and Control*, 3rd ed. Englewood Cliffs, NJ: Prentice-Hall, 2003.
- [31] A. Morawiec, *Orientations and Rotations: Computations in Crystallographic Textures*. New York: Springer, 2003.
- [32] G. F. Franklin, J. D. Powell, and M. Workman, *Digital Control of Dynamic Systems*, 3rd ed. Boston, MA: Addison Wesley, 1998.
- [33] A. H. Jazwinski, *Stochastic Processes and Filtering Theory*. New York: Academic Press, 1970.
- [34] B. D. O. Anderson and J. B. Moore, *Optimal Filtering*. New York: Dover, 1979.
- [35] W. J. Rugh, *Linear System Theory*, 2nd ed. Englewood Cliffs, NJ: Prentice-Hall, 1995.
- [36] D. Goshen-Meskin and I. Y. Bar-Itzhack, "Observability analysis of piece-wise constant systems – Part I: Theory," *IEEE Trans. Aerosp. Electron. Syst.*, vol. 28, no. 10, pp. 1056–1067, Oct. 1992.
- [37] D. Goshen-Meskin and I. Y. Bar-Itzhack, "Observability analysis of piece-wise constant systems—Part II: Application to inertial navigation in-flight alignment," *IEEE Trans. Aerosp. Electron. Syst.*, vol. 28, no. 10, pp. 1068–1075, Oct. 1992.
- [38] P. Batista, C. Silvestre, and P. Oliveira, "Position and velocity navigation filters for marine vehicles," presented at the 17th IFAC World Congr., Seoul, South Korea, Jul. 2008.
- [39] J. C. Gower and G. B. Dijkstra, *Procrustes Problems*. London, U.K.: Oxford Univ. Press, 2004, vol. 30, Oxford Statistical Science Series.
- [40] G. Wahba, "A least-squares estimate of satellite attitude," *SIAM Rev.*, vol. 7, no. 3, pp. 409 problem 65–1, 1965.
- [41] I. Y. Bar-Itzhack and R. R. Harman, "Optimized TRIAD algorithm for attitude determination," *J. Guid., Control, Dyn.*, vol. 20, no. 1, pp. 208–211, Jan. 1997.
- [42] M. J. Caruso, "Applications of magnetoresistive sensors in navigation systems," Honeywell Inc., Plymouth, MN, 1998.
- [43] S. Bittanti, P. Colaneri, and G. Nicolao, "An algebraic Riccati equation for the discrete-time periodic prediction problem," *Syst. Control Lett.*, pp. 71–78, 1990.
- [44] A. V. Oppenheim, R. W. Schaffer, and J. R. Buck, *Discrete-Time Signal Processing*, 2nd ed. Englewood Cliffs, NJ: Prentice-Hall, 1999, Signal Processing.



José F. Vasconcelos (S'06) received the Licenciatura and the Ph.D. degrees in electrical engineering from the Instituto Superior Técnico (IST), Lisbon, Portugal, in 2003 and 2010, respectively.

Since 2009, he has been a Project Engineer with the Advanced Projects Department, Deimos Engenharia, Lisbon, Portugal. His research interests include nonlinear observers, inertial navigation systems, sensor calibration, and robust control with application to autonomous vehicles.

Dr. Vasconcelos was a recipient of two Diploma de

Mérito during his graduation.



Bruno Cardeira received the Licenciatura and the M.Sc. degrees in electrical engineering from the Instituto Superior Técnico (IST), Lisbon, Portugal, in 2003 and 2009, respectively.

He is currently with the Dynamical Systems and Ocean Robotics (DSOR) Laboratory, the Institute for Systems and Robotics (ISR), IST.



Carlos Silvestre (M'07) received the Licenciatura degree in electrical engineering and the M.Sc. degree in electrical engineering and the Ph.D. degree in control science from the Instituto Superior Técnico (IST), Lisbon, Portugal, in 1987, 1991, and 2000, respectively.

Since 2000, he has been with the Department of Electrical Engineering, IST, where he is currently an Assistant Professor of Control and Robotics. Over the past years, he has conducted research in the fields of guidance, navigation, and control of single and multiple air and ocean vehicles. His research interests include linear and nonlinear control theory, coordinated control of multiple vehicles, gain scheduled control, integrated design of guidance and control systems, inertial navigation systems, and mission control and real time architectures for complex autonomous systems with applications to unmanned vehicles.



Paulo Oliveira (M'92) received the Ph.D. degree from the Instituto Superior Técnico (IST), Lisbon, Portugal, in 2002.

He is currently an Assistant Professor with the Department of Electrical and Computer Engineering, IST. He is a Researcher with the Institute for Systems and Robotics—Associate Laboratory, Lisbon. His current research interests include robotics and autonomous vehicles with special focus on the fields of nonlinear estimation, sensor fusion, navigation, positioning, and advanced signal processing techniques.

He has participated in 15 Portuguese and European research projects and is the author of over 100 conference and journal papers.



Pedro Batista (S'09) received the Licenciatura degree in electrical and computer engineering from Instituto Superior Técnico (IST), Lisbon, Portugal, in 2005, where he is currently pursuing the Ph.D. degree in the same field.

From 2004 to 2006, he was Monitor with the Department of Mathematics, IST. His research interests include sensor-based control and navigation of autonomous vehicles.

Mr. Batista was a recipient of the Diploma de Mérito twice during his graduation.